NASA TN D-379

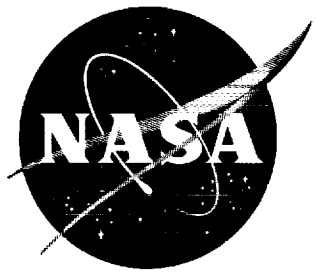

TECHNICAL NOTE

D-379

SUBSONIC KERNEL-FUNCTION FLUTTER ANALYSIS OF A HIGHLY TAPERED TAIL SURFACE AND COMPARISON WITH EXPERIMENTAL RESULTS

By Gerald D. Walberg

Langley Research Center
Langley Field, Va.

NATIONAL AERONAUTICS AND SPACE ADMINISTRATION
WASHINGTON

September 1960

NATIONAL AERONAUTICS AND SPACE ADMINISTRATION

TECHNICAL NOTE D-379

SUBSONIC KERNEL-FUNCTION FLUTTER ANALYSIS OF A HIGHLY TAPERED TAIL SURFACE AND COMPARISON WITH EXPERIMENTAL RESULTS

By Gerald D. Walberg

SUMMARY

A flutter analysis employing the kernel function for three-dimensional, subsonic, compressible flow is applied to a flutter-tested tail surface which has an aspect ratio of 3.5, a taper ratio of 0.15, and a leading-edge sweep of 30°. Theoretical and experimental results are compared at Mach numbers from 0.75 to 0.98. Good agreement between theoretical and experimental flutter dynamic pressures and frequencies is achieved at Mach numbers to 0.92. At Mach numbers from 0.92 to 0.98, however, a second solution to the flutter determinant results in a spurious theoretical flutter boundary which is at a much lower dynamic pressure and at a much higher frequency than the experimental boundary.

INTRODUCTION

In order to predict successfully the flutter characteristics of a low-aspect-ratio, plate-like lifting surface, a flutter analysis must employ accurate, three-dimensional, aerodynamic forces. Because of the prominent role of flutter in modern airplane design, the development of practical procedures for calculating three-dimensional, unsteady, aerodynamic forces is a problem of increasing importance.

A promising approach to this problem involves direct consideration of the integral equation relating the lift and downwash distributions of oscillating finite wings. Basic to the solution of this equation is the evaluation of its kernel, a function which is essentially an aerodynamic influence coefficient representing the downwash at some point on a lifting surface due to a unit aerodynamic load at any other point on the surface. In reference 1, the kernel function for oscillating finite wings in compressible subsonic flow was reduced to a form which could be conveniently evaluated. By using this form of the kernel, a subsonic lifting-surface method for calculating the forces on a harmonically oscillating wing of arbitrary plan form and deflection mode

was developed in reference 2. This method employed a systematic numerical solution of the integral equation and was suitable for programing in high-speed computing machines.

In reference 3, the lifting-surface method of reference 2 was employed in a modal-type flutter analysis. This flutter analysis appears to be well suited to the study of thin low-aspect-ratio surfaces at subsonic speeds, since it is capable of accounting for the effects of compressibility, finite span, and chordwise deformation. Few comparisons between flutter boundaries, calculated by this analysis, and experimental flutter boundaries are presently available. The purpose of the present paper is to present such a comparison.

In the present investigation a tail surface having an aspect ratio of 3.5 and a taper ratio of 0.15 was flutter tested at Mach numbers from 0.75 to 1.06. This model had a leading-edge sweep of 30° and a 3.5-percent-thick biconvex section. The natural vibration modes of the model involved significant chordwise deformation. Theoretical flutter boundaries were calculated, for Mach numbers from 0 to 0.98, by using the analysis of reference 3 (with minor modifications). In the analysis, the flutter mode was approximated by a linear combination of the first three experimentally measured natural vibration modes of the model. Theoretical and experimental flutter boundaries are compared herein.

L 6 1 5

SYMBOLS

A	aspect ratio
A_p	panel aspect ratio
A_{ij}	generalized aerodynamic force $\frac{1}{b_0 l} \iint_S h_i L_j \, dS$
b_0	streamwise root semichord, ft
b_t	streamwise tip semichord, ft
f	frequency of vibration, cps
f_i	frequency of the ith natural vibration mode, cps
g	structural damping coefficient

$h(x,y,t)$	instantaneous deflection of point on tail surface in flutter mode, ft
h_i	displacement of point x,y in the ith mode of vibration normalized with respect to the maximum displacement in that mode $h_i(x,y)$
I	imaginary part of complex unknown Ω
i,j	indices denoting a particular natural vibration mode
k_0	reduced frequency, $b_0\omega/V$
l	exposed semispan, ft
L_j	dimensionless series expression for aerodynamic load distribution due to motion in jth vibration mode
M	Mach number
M_i	generalized mass associated with ith mode of vibration $\iint_S m(x,y)h_i^2 dS$, slugs
$m(x,y)$	local mass per unit area at point x,y, slugs/sq ft
q	dynamic pressure, lb/sq ft
Q_i	generalized force associated with ith mode of vibration, lb
q_i	generalized coordinate in ith mode of vibration, $\bar{q}_i e^{i\omega t}$, ft
$\bar{q}_i$	complex amplitude of generalized coordinate in ith mode, ft
R	real part of complex unknown Ω
S	surface area of tail, sq ft
t	time, sec
V	velocity of airstream, ft/sec
x,y,z	cartesian coordinates (see fig. 4)
θ	angular chordwise variable (see fig. 5)

Λ_{LE} leading-edge sweep angle, deg

λ taper ratio

λ_p panel taper ratio

μ panel mass ratio, ratio of exposed panel mass to mass of a truncated cone of air having lower base diameter $2b_0$, upper base diameter $2b_t$, and height l

μ_i generalized mass in ith mode of vibration referred to a density parameter, $4\pi\rho l^2 b_0$ (see eq. (11))

ρ density of airstream, slugs/cu ft

Ω complex unknown of flutter determinant, $\left(\frac{\omega_i}{\omega}\right)^2(1 + ig)$

ω angular frequency, $2\pi f$, radians/sec

ω_i angular frequency of ith vibration mode, $2\pi f_i$, radians/sec

Dots over symbol indicate derivatives with respect to time.

EXPERIMENTAL INVESTIGATION

Model Geometry and Construction

The experimental data, presented herein, were obtained from one of a series of all-movable, horizontal stabilizers which were flutter tested in the Langley 8-foot transonic pressure tunnel. The model used for the present investigation had an aspect ratio of 3.5, a taper ratio of 0.15, a leading-edge sweep of 30°, and a 3.5-percent-thick biconvex section. Structural and geometric details of the model are shown in table I and in figure 1.

As shown in figure 1, the model was built up of 0.010-inch-thick duralumin laminations. These laminations were covered with balsa which was shaped to the desired external contour. The outer surface of the model was covered with a thin plastic film. Incorporated in the model center section were two ball-bearing trunnions which located the hinge line at 40 percent of the mean aerodynamic chord. For the present investigation, however, the actuator rib (see fig. 1) was clamped to

prevent its rotation about the hinge line. This clamping of the center section served to increase the amount of chordwise deformation involved in the natural vibration modes of the model.

Physical Properties of Model

The natural frequencies of vibration were determined by exciting the model with two electromagnetic shakers located fore and aft near the root chord. During these vibration tests, the model was mounted in the wind tunnel exactly as it would be mounted for the flutter tests which were to follow. Time-exposure photographs were employed to determine the natural vibration modes of the model. These photographs were taken with a camera which was mounted outboard of the model tip and directed spanwise toward the root. The upper surface of one panel of the model was painted flat black and had thin, white, chordwise lines located at every one-tenth of the exposed semispan. With the model moving in one of its natural modes, a time-exposure photograph was taken. In the photograph, the chordwise white lines appeared as bands, the thickness of these bands being indicative of the amplitude of motion. The first three natural modes and their frequencies are presented in figure 3.

Instrumentation

The model was instrumented with electrical strain gages. Two groups of gages were used on each panel of the model. The first group, which consisted of bending and torsion gages bonded to both the upper and lower panel surface, was located near the 50-percent-chord line and the panel root. The second group consisted of torsion gages bonded to the upper panel surface and was located near the 50-percent-chord line at 70 percent of the exposed semispan. During the tests, a recording oscillograph was used to record the signals from the various gages. These records were used to determine flutter frequencies and the onset of flutter. The strain-gage signals were also fed into a cathode-ray oscilloscope in such a way that a Lissajous pattern indicated the start of flutter. At each test point, the tunnel Mach number, stagnation temperature, and stagnation pressure were recorded by a punchcard readout system.

Tunnel and Support System

The tests were conducted in the Langley 8-foot transonic pressure tunnel which is a single-return tunnel having a rectangular, slotted throat. In this tunnel, stagnation pressure and Mach number are

independently variable. Some details of the tunnel test section have been presented in reference 4.

The model was mounted at an angle of attack of 0° on a long, 5.5-inch-diameter cylindrical fuselage which extended into the subsonic region upstream of the test section. The fuselage was considered a rigid mount, since the fuselage mass was many times greater than the model mass. The measured fundamental vibration frequency of the support system was 4.3 cycles per second.

Flutter Tests

Experimental zero-lift flutter points were obtained at Mach numbers from 0.75 to 1.06. The procedure used in obtaining flutter at a given Mach number was to increase stagnation pressure gradually until flutter was obtained. After flutter was obtained, tunnel conditions were held constant momentarily and then Mach number and stagnation pressure were reduced as rapidly as possible in an effort to save the model from destruction. All flutter points reported herein were obtained from the same model. Experimental results are presented in table II.

ANALYTICAL INVESTIGATION

This section presents the method of flutter analysis used in the present investigation. Because of the similarity between the present analysis and that of reference 3, the method is described only in general terms.

In the present analysis, the fuselage side was assumed to act as a reflection plane. Hence, the plan form which was analyzed is that plan form which results if, in figure 1, the center section is removed and the panels are joined along their respective root chords. This resultant plan form and the coordinate system used in the analysis are presented in figure 4.

Equations of Motion

In the present analysis, the flutter mode is approximated by a linear combination of the model's first three natural (orthogonal) vibration modes; that is,

$$h(x,y,t) = q_1(t)h_1(x,y) + q_2(t)h_2(x,y) + q_3(t)h_3(x,y) \qquad (1)$$

where $q_i(t) = \bar{q}_i e^{i\omega t}$ is the generalized coordinate for the ith degree of freedom and $h_i(x,y)$ is the associated normalized natural mode shape.

If the Lagrangian formulation is applied and the procedure of reference 3 is followed, the resulting equation of motion for the ith degree of freedom is of the form

$$M_i \ddot{q}_i + \omega_i^2 M_i q_i = Q_i \tag{2}$$

L 6 1 5

where M_i and Q_i are, respectively, the generalized mass and the generalized aerodynamic force for the ith degree of freedom. If the definition $q_i = \bar{q}_i e^{i\omega t}$ is employed, equation (2) may be written in the form

$$\left[1 - \left(\frac{\omega_i}{\omega}\right)^2\right] M_i q_i + \frac{1}{\omega^2} Q_i = 0 \tag{3}$$

which corresponds to equation (6) of reference 3.

Generalized Mass

The generalized mass for the ith degree of freedom is defined as

$$M_i = \iint_S m(x,y) h_i^2 dS \tag{4}$$

where $m(x,y)$ is the distribution of wing mass per unit area, and h_i is the ith normalized, natural mode shape. In the present investigation, both $m(x,y)$ and h_i were determined experimentally, as described in the section entitled "Physical Properties of Model." In order to evaluate M_i, the wing was divided into 27 mass elements, and the displacement of the center of mass of each element $h_i^{(k)}$ was taken from the appropriate mode shape. The generalized mass for the ith mode was then computed as

$$M_i = \sum_{k=1}^{27} m^{(k)} \left[h_i^{(k)}\right]^2 \tag{5}$$

where $m^{(k)}$ is the mass of the kth element.

Generalized Aerodynamic Force

As shown in reference 3, the generalized aerodynamic force may be expressed as

$$\frac{1}{\omega^2} Q_i = \frac{4\pi\rho V^2 l}{b_0^2 \omega^2} \left(\bar{q}_1 \iint_S h_i L_1 \, dS + \bar{q}_2 \iint_S h_i L_2 \, dS + \bar{q}_3 \iint_S h_i L_3 \, dS \right) \tag{6}$$

In equation (6), L_j is a series expression for the aerodynamic load distribution due to motion in the jth natural mode. Basically, two steps are required in the calculation of Q_i. The first step is the determination of L_j and the second step is the evaluation of the surface integrals $\iint_S h_i L_j \, dS$. Reference 2 describes a collocation procedure which is used to determine L_j. This procedure consists of representing the aerodynamic surface loading by a series expression that automatically satisfies the conditions of load at the wing edges. The downwash angles at various control points on the surface are then used as boundary conditions to determine the values of the arbitrary coefficients in the assumed series. The locations of the control points used in the present investigation are shown in figure 5. After L_j is determined, the evaluation of Q_i is simply a matter of performing the surface integrations $\iint_S h_i L_j \, dS$. In the present investigation, this integration was performed numerically by using an 11-point Simpson's Rule in the spanwise direction and a 9-point Simpson's Rule in the chordwise direction. The numerical integration lattice is shown in figure 5.

L
6
1
5

Flutter Determinant

By substituting equation (6) into equation (3), the ith equation of motion may be written in the form

$$\left[1 - \left(\frac{\omega_i}{\omega} \right)^2 \right] \bar{q}_i + \frac{4\pi\rho V^2 l}{M_i b_0^2 \omega^2} \left(\bar{q}_1 \iint_S h_i L_1 \, dS + \bar{q}_2 \iint_S h_i L_2 \, dS + \bar{q}_3 \iint_S h_i L_3 \, dS \right) = 0 \tag{7}$$

or alternatively,

$$\left[1 - \left(\frac{\omega_i}{\omega}\right)^2\right]\bar{q}_i + \frac{1}{k_0^2\mu_i}\left(\bar{q}_1 A_{i1} + \bar{q}_2 A_{i2} + \bar{q}_3 A_{i3}\right) = 0 \tag{8}$$

where

$$A_{ij} = \frac{1}{b_0 l}\iint_S h_i L_j \, dS \tag{9}$$

L
6
1
5

$$k_0 = \frac{b_0\omega}{V} \tag{10}$$

$$\frac{1}{\mu_i} = \frac{4\pi\rho l^2 b_0}{M_i} \tag{11}$$

If equation (8) is written for the three degrees of freedom (natural modes) under consideration, a set of three simultaneous homogeneous equations results. If these equations are to have a nontrivial solution, their coefficient determinant must vanish.

Hence,

$$\begin{vmatrix} 1 - \left(\frac{\omega_1}{\omega_2}\right)^2\Omega + \frac{A_{11}}{k_0^2\mu_1} & \frac{A_{12}}{k_0^2\mu_1} & \frac{A_{13}}{k_0^2\mu_1} \\ \frac{A_{21}}{k_0^2\mu_2} & 1 - \left(\frac{\omega_2}{\omega_2}\right)^2\Omega + \frac{A_{22}}{k_0^2\mu_2} & \frac{A_{23}}{k_0^2\mu_2} \\ \frac{A_{31}}{k_0^2\mu_3} & \frac{A_{32}}{k_0^2\mu_3} & 1 - \left(\frac{\omega_3}{\omega_2}\right)^2\Omega + \frac{A_{33}}{k_0^2\mu_3} \end{vmatrix} = 0 \tag{12}$$

where the complex eigenvalue Ω is defined by

$$\Omega = \left(\frac{\omega_2}{\omega}\right)^2(1 + ig) \tag{13}$$

In this definition of Ω, ω is the unknown frequency and g is a damping coefficient that becomes zero at the borderline condition between damped and undamped motion.

Determination of Theoretical Flutter Boundaries

In the present investigation, theoretical flutter characteristics were determined for Mach numbers M from 0 to 0.98 and mass ratios μ from 20 to 100 by the following procedure.

For each combination of M and μ, the flutter determinant was solved for a range of reduced frequencies k_0. Since expansion of the flutter determinant results in a cubic equation in the complex unknown Ω, each combination of M, μ, and k_0 yields three values of Ω which must be examined to see whether they meet the requirements for a flutter point. By definition,

$$\Omega = \left(\frac{\omega_2}{\omega}\right)^2 (1 + ig) = R + iI$$

therefore,

$$\frac{\omega}{\omega_2} = \frac{1}{\sqrt{R}} \quad \text{and} \quad g = \frac{I}{R}$$

At each M, flutter characteristics were determined from plots of g and ω/ω_2 against $1/k_0$ in which μ was a parameter. Flutter points were taken as being those points where $g = 0$ and $\left(\frac{\omega}{\omega_2}\right)^2 > 0$. As illustrations, curves of g and ω/ω_2 against $1/k_0$ are presented in figures 6 and 7, respectively. The resulting flutter characteristics were plotted as flutter boundaries of dynamic pressure q required for flutter and flutter frequency ratio ω/ω_2 as functions of M with μ as a parameter. Theoretical flutter boundaries corresponding to wind-tunnel conditions were calculated for comparison with the experimental flutter points.

DISCUSSION OF RESULTS

The g against $1/k_0$ and ω/ω_2 against $1/k_0$ curves of figures 6 and 7, respectively, are presented to illustrate the behavior of the flutter determinant roots at various Mach numbers. In the

present investigation, the behavior of these roots was found to be similar throughout the Mach number range $0 \leqq M \leqq 0.90$. Therefore, curves are presented only for $M = 0$, 0.75, and 0.90. These curves show that, for the range $0 \leqq M \leqq 0.90$, the only critical root is that one associated with the second natural mode. It should be noted, however, that, as the Mach number approaches 0.90, the third-mode root approaches the $g = 0$ line.

At a Mach number of 0.92 the character of the determinant roots has changed. At this Mach number, the first- and third-mode roots are both critical. The first-mode root predicts flutter for the mass-ratio range from 20 to 100 and the third-mode root predicts flutter for mass ratios 60 to 100. From figure 6(d) it is seen that the third-mode root loops up over the $g = 0$ line and then continues on the negative side. Hence, the third-mode root indicates flutter over a limited range of $1/k_0$ and μ, whereas the first-mode root indicates flutter for all $1/k_0$ greater than that value for which $g = 0$ and for $20 \leqq \mu \leqq 100$.

At Mach numbers of 0.94, 0.96, and 0.98, the first- and third-mode roots remain critical. The principal effect of an increase in M from 0.92 to 0.98 is that the flutter region predicted by the third-mode root grows until, at $M = 0.98$, only a lower limit on $1/k_0$ is indicated within the reduced-frequency range investigated.

Figure 8 presents theoretical flutter boundaries of dynamic pressure q required for flutter and flutter frequency ratio ω/ω_2 as functions of Mach number with mass ratio as a parameter. Figure 8 shows that the flutter points taken from the first and second-mode roots of the flutter determinant form smooth boundaries. These boundaries, which are shown as solid lines in figure 8, are determined by second-mode-root flutter points at $0 \leqq M \leqq 0.90$ and by first-mode-root flutter points at $0.90 < M \leqq 0.98$. As mentioned previously, the third-mode roots of the flutter determinant also yield flutter points at Mach numbers from 0.92 to 0.98. The flutter boundaries due to these points are shown, in figure 8, as dashed lines. In figures 6 and 7 it was seen that the third-mode roots of the flutter determinant indicated flutter over limited ranges of reduced frequency and mass ratio at Mach numbers from 0.92 to 0.96. Hence, at these Mach numbers an upper and lower boundary of q and ω/ω_2 would exist for each μ. In figure 8, only the lower boundaries are shown. The curves of figure 8 show that, throughout the range of variables investigated, flutter q for a given M varies with μ (and hence with density). Therefore, these theoretical results do not agree with the so-called constant-q concept of flutter. However, the variation of q with μ becomes small at high μ. The effect of μ on the variation of q with M is also of interest. Consider the first- and second-mode-root curves. For a μ of 20, q decreases slowly as M goes from 0 to 0.90 and then increases

abruptly for $M > 0.90$. For $\mu = 40$, the decrease in q with increasing M is greater than for $\mu = 20$, and the minimum value of q is reached at $M = 0.925$. In general, figure 8 shows that, as μ increases, the decrease in q with increasing M becomes more pronounced, and the minimum value of q occurs at a higher M. These trends bear a remarkable similarity to the trends of experimental data presented in figure 21 of reference 5.

In figure 9, the theoretical and experimental results of the present investigation are compared. The theoretical curves of figure 9 were obtained from calculations employing the experimental value of μ for each M. Figure 9 shows that, for M from 0.75 to 0.92, the agreement between theory and experiment is good for both q and ω/ω_2. For M from 0.92 to 0.98, however, two theoretical flutter boundaries exist. In flutter prediction by theoretical means, the flutter solution which yields the lowest q must be accepted at each Mach number. Hence, on this basis, the third-mode-root boundary, which predicts a flutter frequency very near the frequency of the third natural vibration mode, must be accepted for $0.92 \leqq M \leqq 0.98$. For this boundary the agreement of both q and ω/ω_2 with experimental results is poor. If, however, the third-mode root were disregarded, the agreement between theory and experiment, especially with regard to trends, would be acceptable for the entire M range for which calculations were made. There is, however, no reasonable basis for disregarding the third-mode-root flutter. The operating path of the wind tunnel was such that, if this flutter had existed physically, it would have been encountered during the experimental investigation.

L 6 1 5

In an attempt to determine the origin of the third-mode-root flutter, some calculations were undertaken for $M = 0.94$ in which various two-degree-of-freedom subcases of the flutter determinant were examined. When the first two natural vibration modes were considered, only the flutter solution which gave acceptable agreement with experiment was obtained. The third-mode-root flutter was found only when a combination of the second and third natural modes was used. It is noted that the frequencies of these modes are very close together; this in itself might be expected to lead to conditions of resonance. Since no such flutter as that indicated by the third-mode root was found experimentally, it may be concluded that this flutter mode is sensitive to some factor not properly accounted for in the analysis. A complete understanding of the nature of this additional flutter solution would require a broad survey of the many factors which might possibly influence it. Such a survey would include considerations of various control point locations and numerical integration techniques, of higher structural modes, and of structural damping.

CONCLUDING REMARKS

A flutter analysis employing the kernel function for three-dimensional, compressible flow was applied to a flutter-tested tail surface which had an aspect ratio of 3.5, a taper ratio of 0.15, and a leading-edge sweep of 30°. The flutter tests covered the Mach number range from 0.75 to 1.06. Theoretical flutter boundaries were calculated for Mach numbers from 0 to 0.98. In the calculations, the flutter mode was approximated by a linear combination of the first three natural vibration modes of the model.

L
6
1
5

Good agreement between theoretical and experimental flutter dynamic pressures and frequencies was achieved for Mach numbers up to 0.92. At Mach numbers from 0.92 to 0.98, a second solution to the flutter determinant resulted in spurious theoretical flutter points which were at a much lower dynamic pressure and a much higher frequency than the experimental points.

Langley Research Center,
National Aeronautics and Space Administration,
Langley Field, Va., February 11, 1960.

REFERENCES

1. Watkins, Charles E., Runyan, Harry L., and Woolston, Donald S.: On the Kernel Function of the Integral Equation Relating the Lift and Downwash Distributions of Oscillating Finite Wings in Subsonic Flow. NACA Rep. 1234, 1955. (Supersedes NACA TN 3131.)

2. Watkins, Charles E., Woolston, Donald S., and Cunningham, Herbert J.: A Systematic Kernel Function Procedure for Determining Aerodynamic Forces on Oscillating or Steady Finite Wings at Subsonic Speeds. NASA TR R-48, 1959.

3. Woolston, Donald S., and Sewall, John L.: Use of the Kernel Function in a Three-Dimensional Flutter Analysis With Application to a Flutter-Tested Delta-Wing Model. NACA TN 4395, 1958.

4. Mugler, John P., Jr.: Transonic Wind-Tunnel Investigation of the Aerodynamic Loading Characteristics of a 60° Delta Wing in the Presence of a Body With and Without Indentation. NACA RM L55G11, 1955.

5. Maier, Henry G., and King, Stephen R.: Transonic Flutter Model Tests - Part I. 45 Degree Swept Wings. WADC Tech. Rep. 56-214, Pt. I, ASTIA Doc. No. AD131067, U.S. Air Force, Sept. 1957.

TABLE I

PROPERTIES OF MODEL

Aspect ratio, A	3.5
Thickness ratio	0.035
Taper ratio, λ	0.15
Leading-edge sweep angle, Λ_{LE}, deg	30
Streamwise airfoil section	Biconvex
Streamwise root semichord, b_0, ft	0.625
Exposed semispan, l, ft	1.22
Exposed panel mass, lb-sec^2/ft	0.055
Panel aspect ratio, A_p	1.66
Panel taper ratio, λ_p	0.176
Natural frequencies, cps:	
First mode	40
Second mode	108
Third mode	117

TABLE II

EXPERIMENTAL FLUTTER POINTS

Point	M	V, ft/sec	ρ, lb-sec^2/ft^4	q, lb/sq ft	f, cps	ω, rad/sec	ω/ω_2	μ
1	0.750	841.7	0.002146	760	64.1	402	0.592	44.3
2	.848	938.5	.001509	664	57.4	360	.531	63.0
3	.912	1,001.3	.001197	600	51.9	325	.479	79.5
4	.958	1,044.1	.001114	607	54.9	344	.507	85.4
5	.983	1,067.0	.001232	701	56.5	354	.522	77.2
6	1.060	1,135.7	.001114	718	56.1	352	.519	85.4

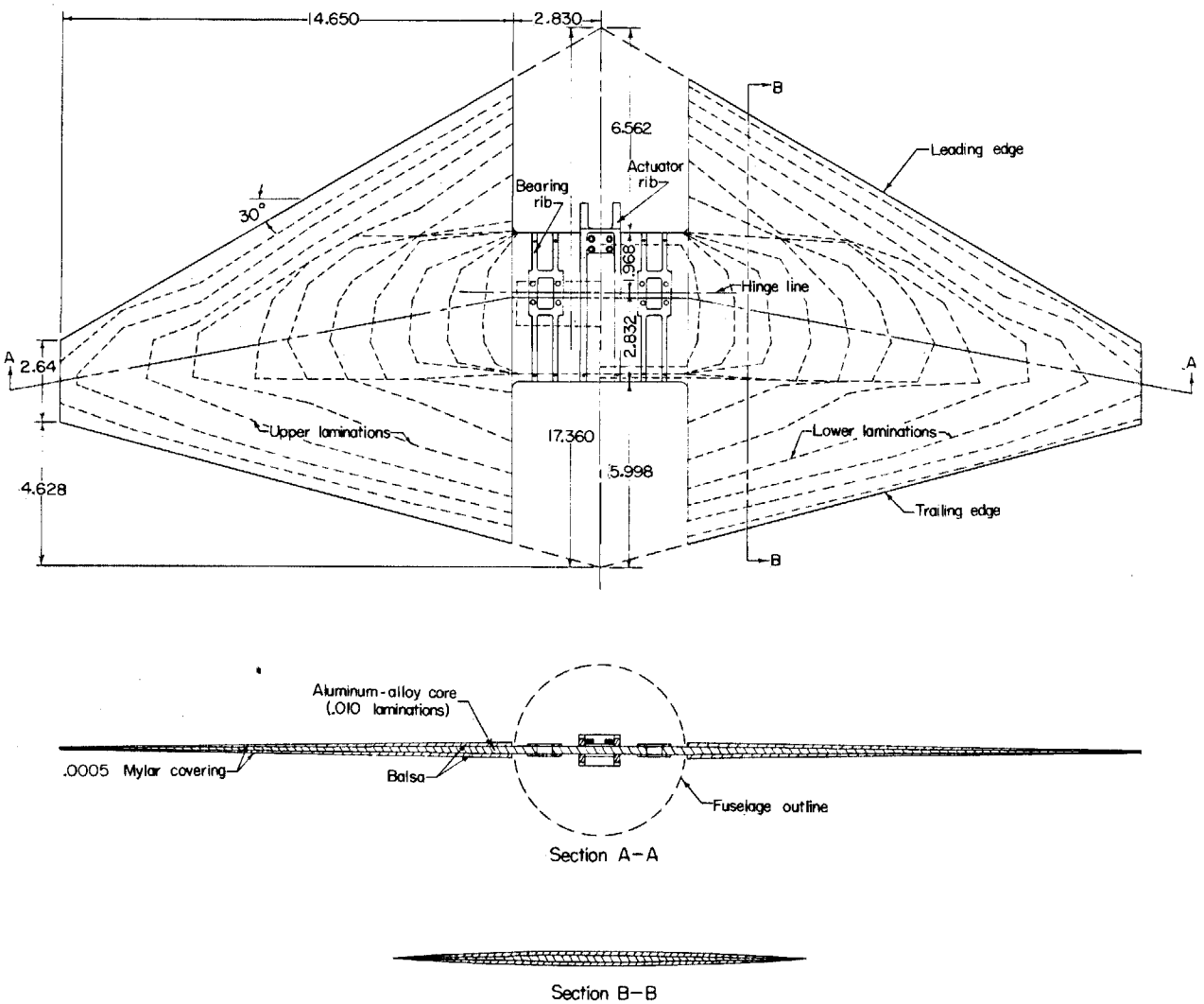

Figure 1.- Structural and geometric details of model. All dimensions are in inches unless otherwise specified.

MASS ELEMENTS

No.	Mass, $\frac{\text{lb-sec}^2}{\text{ft}}$	Center of mass location	
		y/l	x/b_0
1	0.00118	0.103	-0.778
2	.00252	.058	-.514
3	.00485	.089	-.232
4	.00307	.088	-.008
5	.00422	.089	.190
6	.00432	.093	.482
7	.00143	.099	.793
8	.00127	.333	-.507
9	.00053	.255	-.427
10	.00484	.321	-.226
11	.00323	.321	-.010
12	.00463	.324	.187
13	.00329	.320	.452
14	.00140	.321	.715
15	.00103	.580	-.183
16	.00326	.545	-.032
17	.00379	.579	.198
18	.00248	.572	.412
19	.00090	.571	.627
20	.00044	.774	-.008
21	.00093	.772	.197
22	.00053	.774	.387
23	.00031	.774	.540
24	.00025	.914	.113
25	.00050	.916	.241
26	.00037	.922	.371
27	.00022	.922	.490

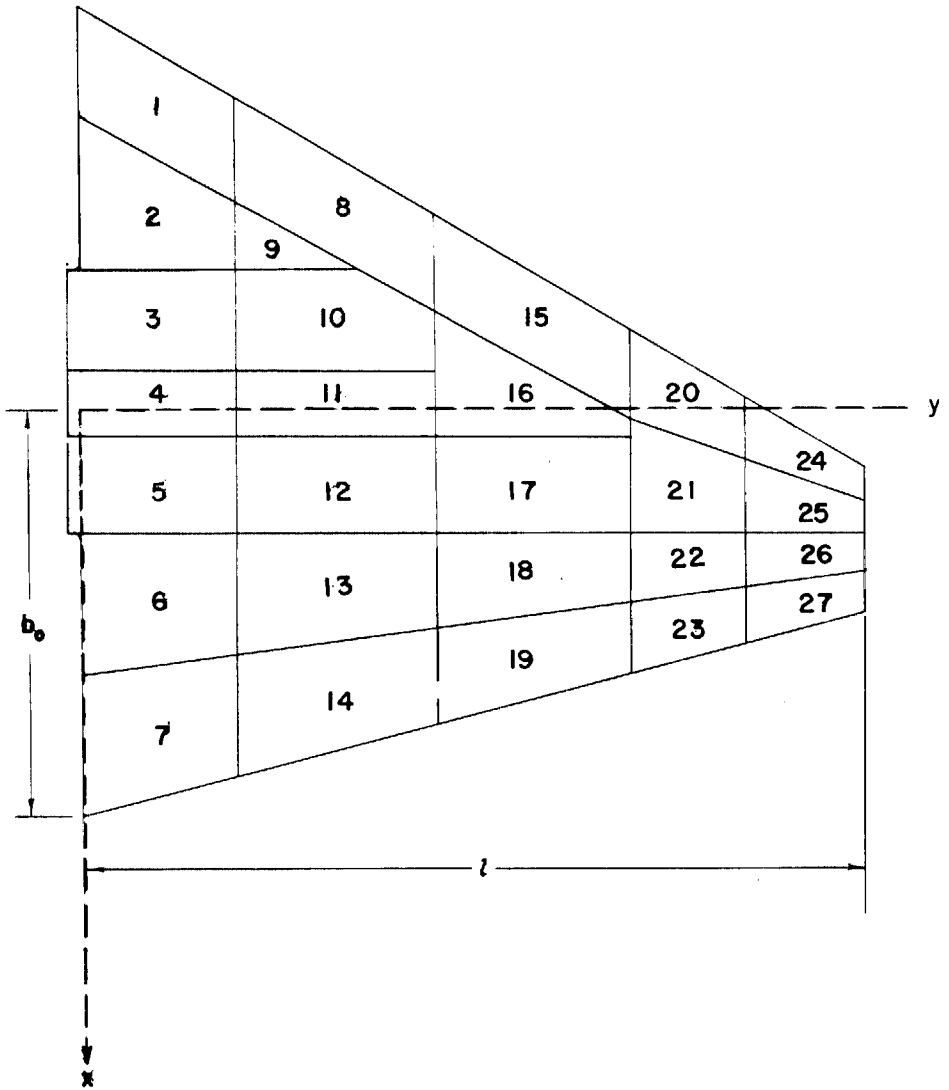

Figure 2.- Mass distribution of model.

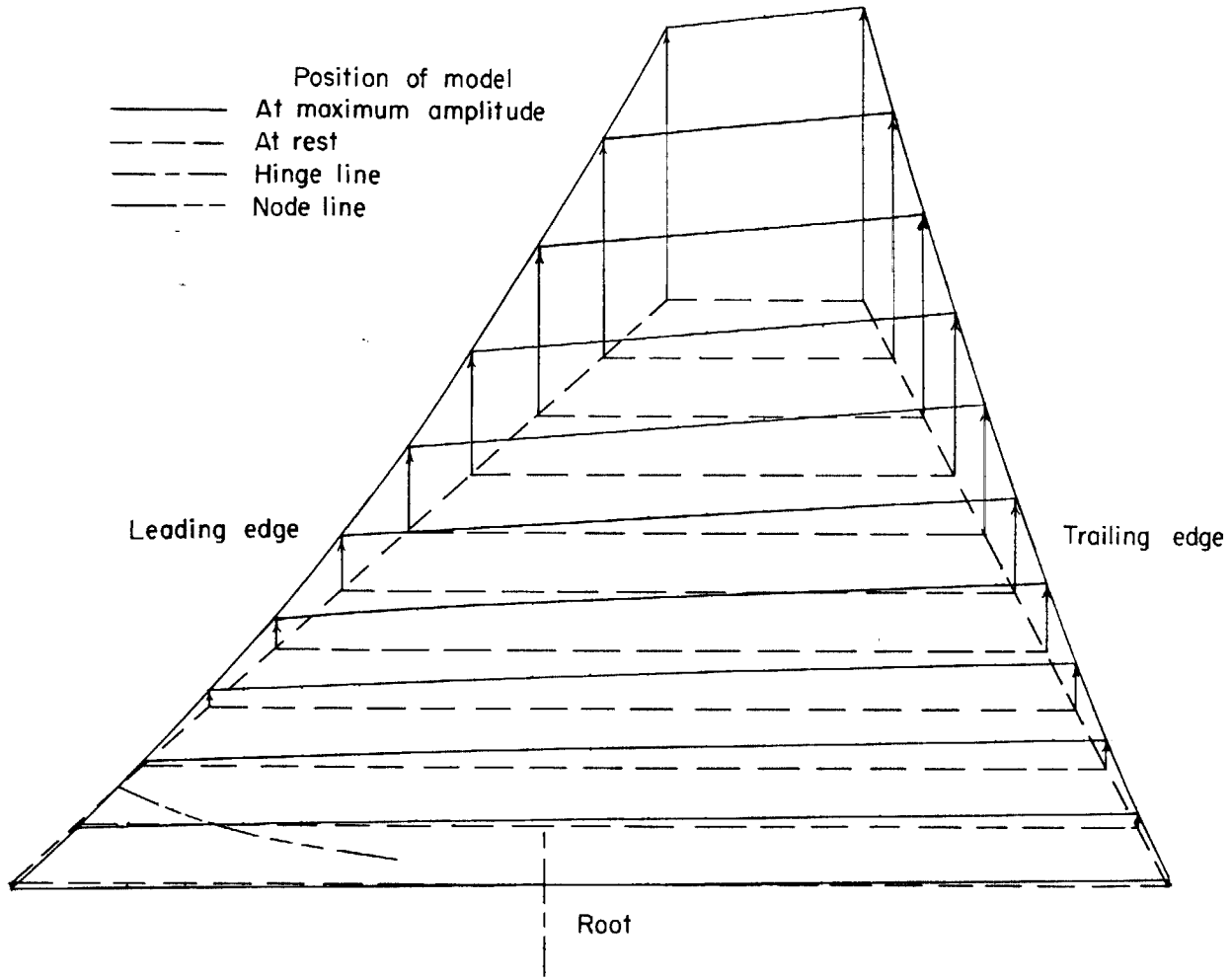

(a) First mode; f_1 = 40 cps.

Figure 3.- Experimentally determined natural mode shapes.

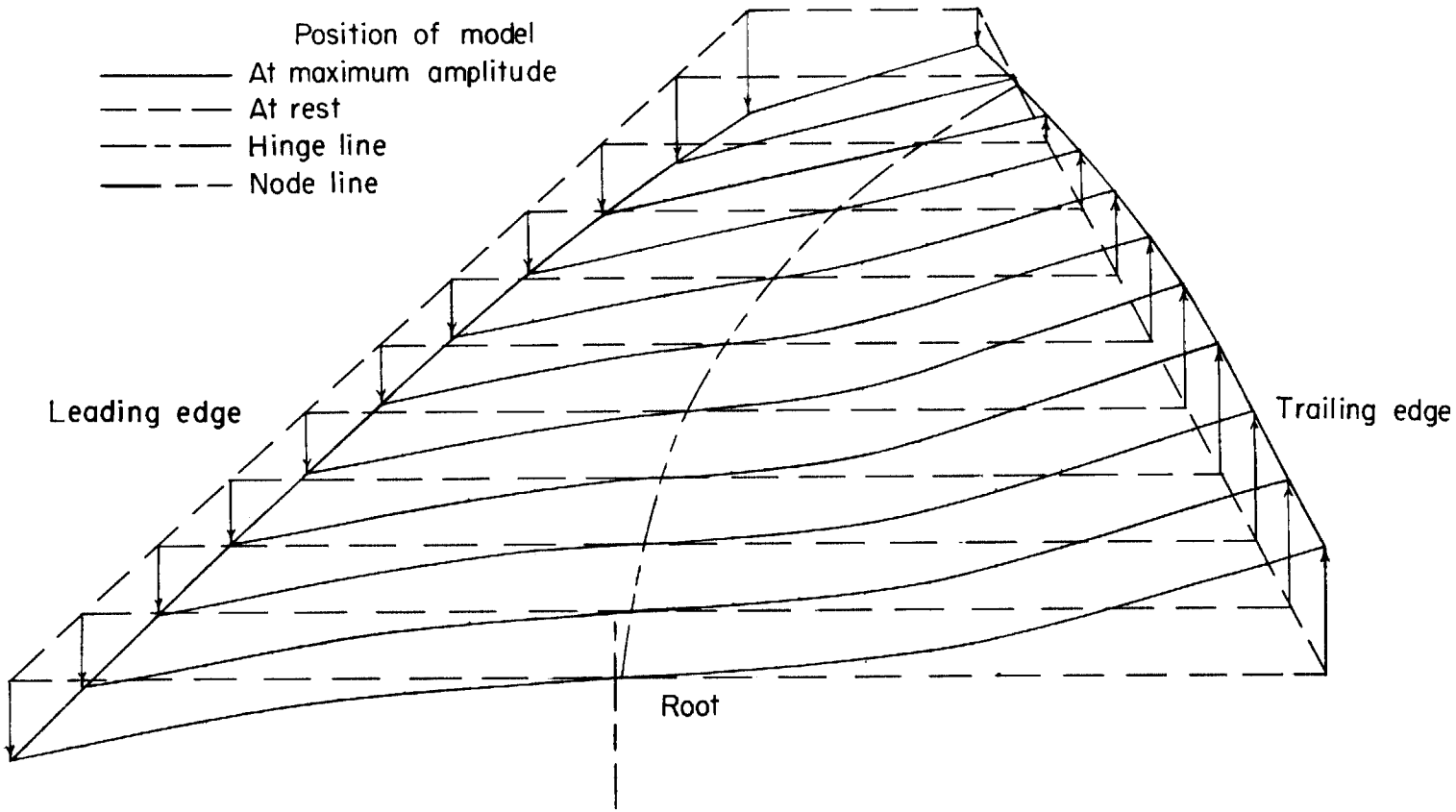

(b) Second mode; f_2 = 108 cps.

Figure 3.- Continued.

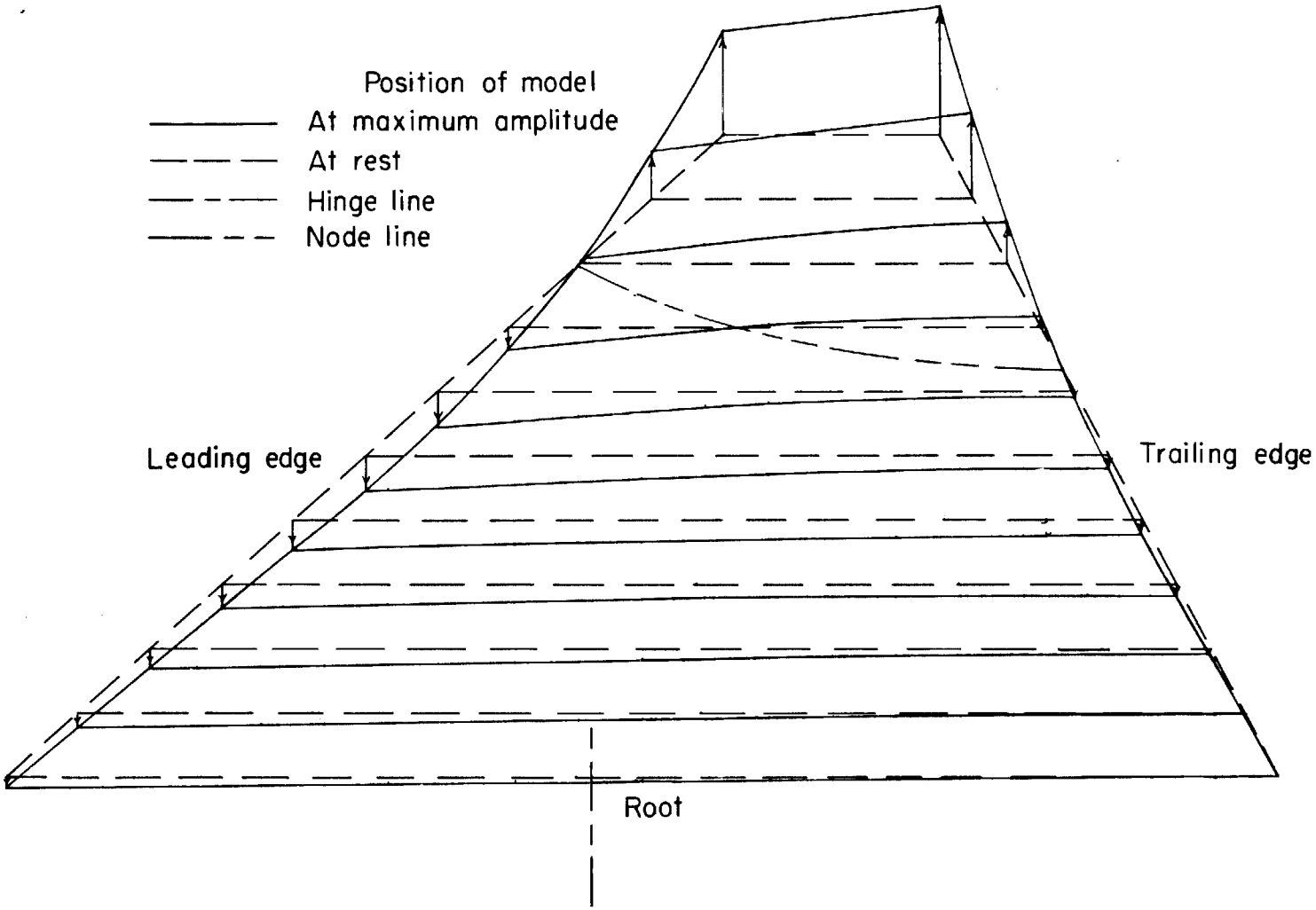

(c) Third mode; f_3 = 117 cps.

Figure 3.- Concluded.

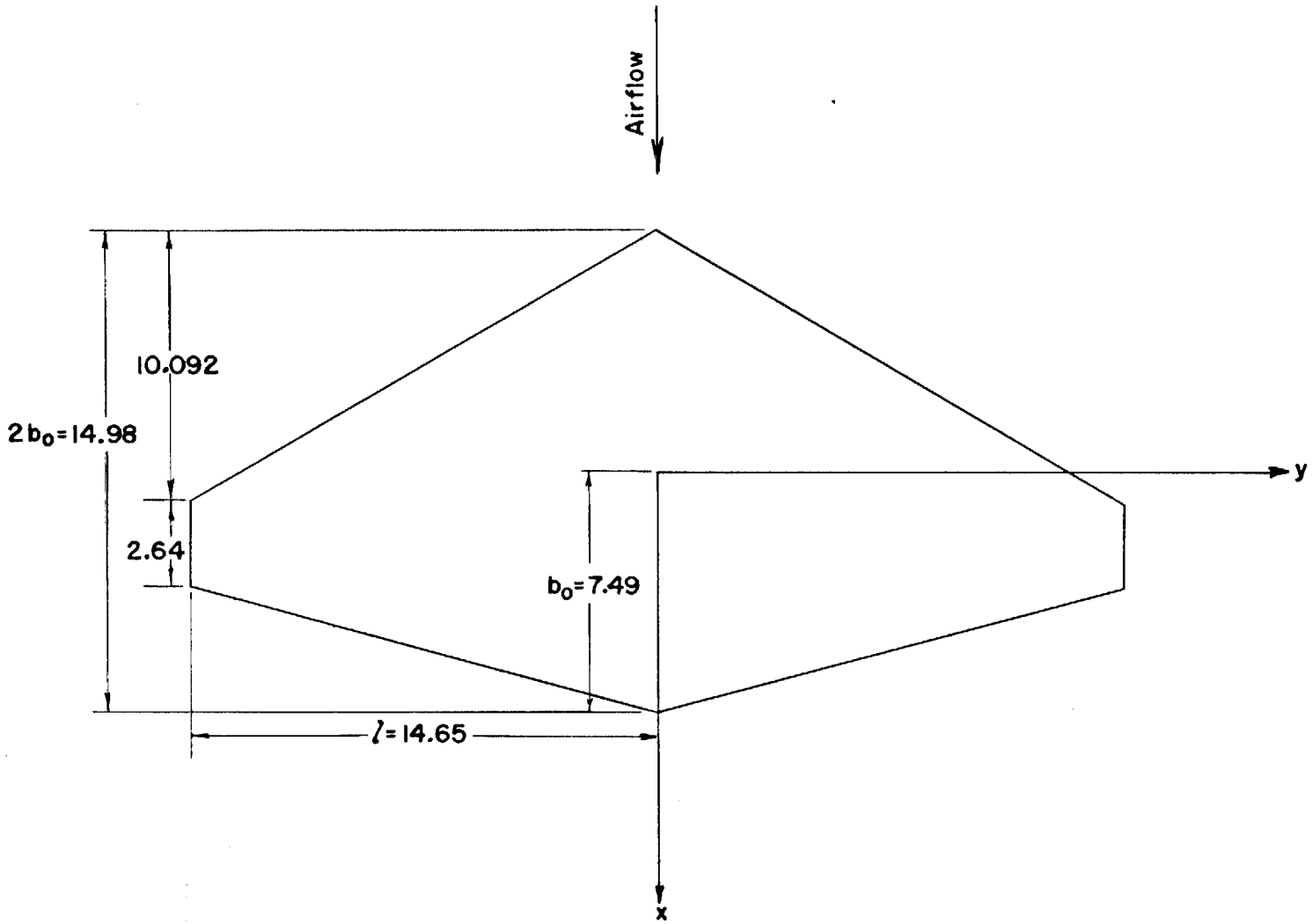

Figure 4.- Plan form and coordinate system used in theoretical investigation. All dimensions are in inches. Note: z positive downward.

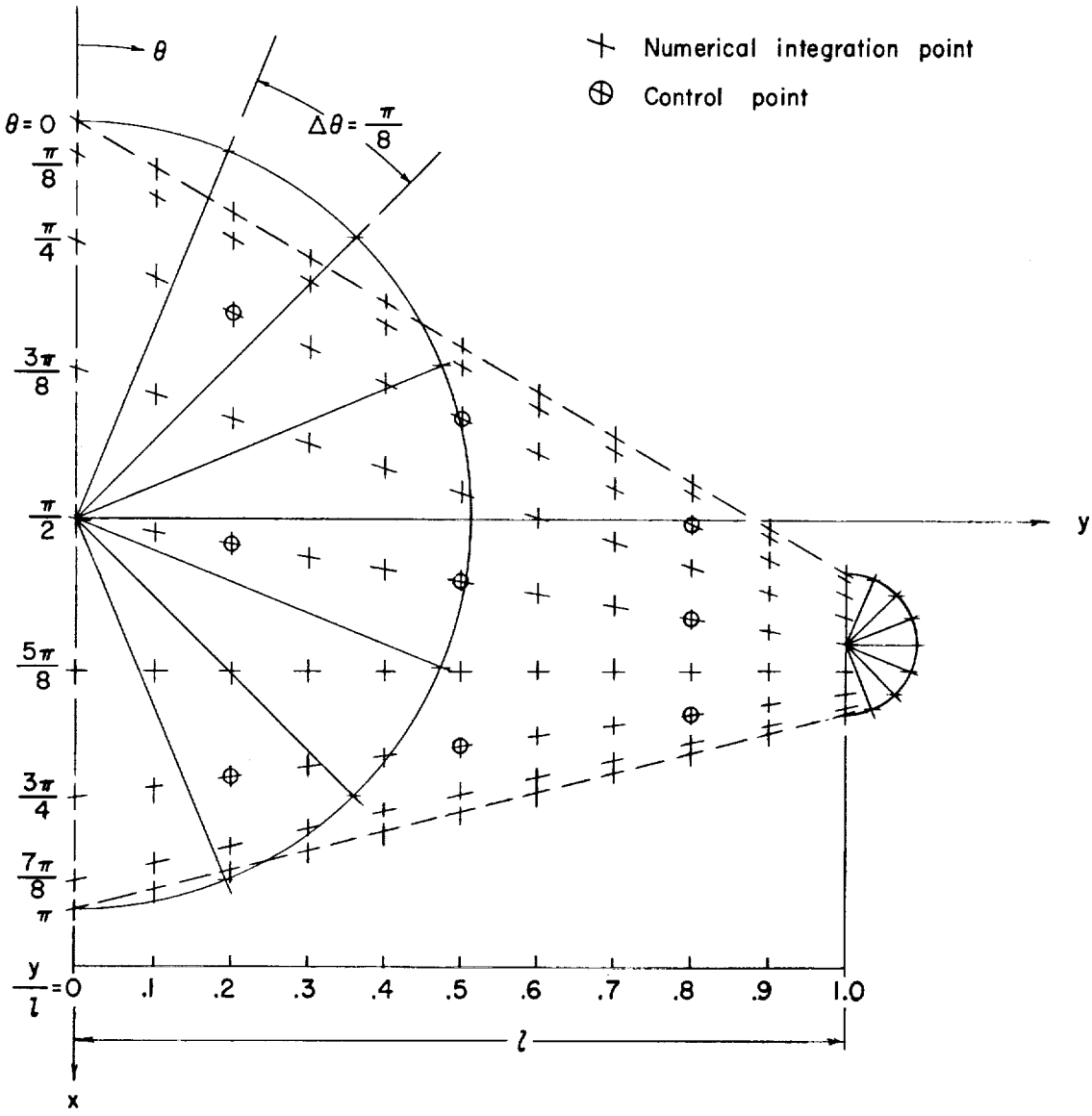

Figure 5.- Control points and numerical integration points.

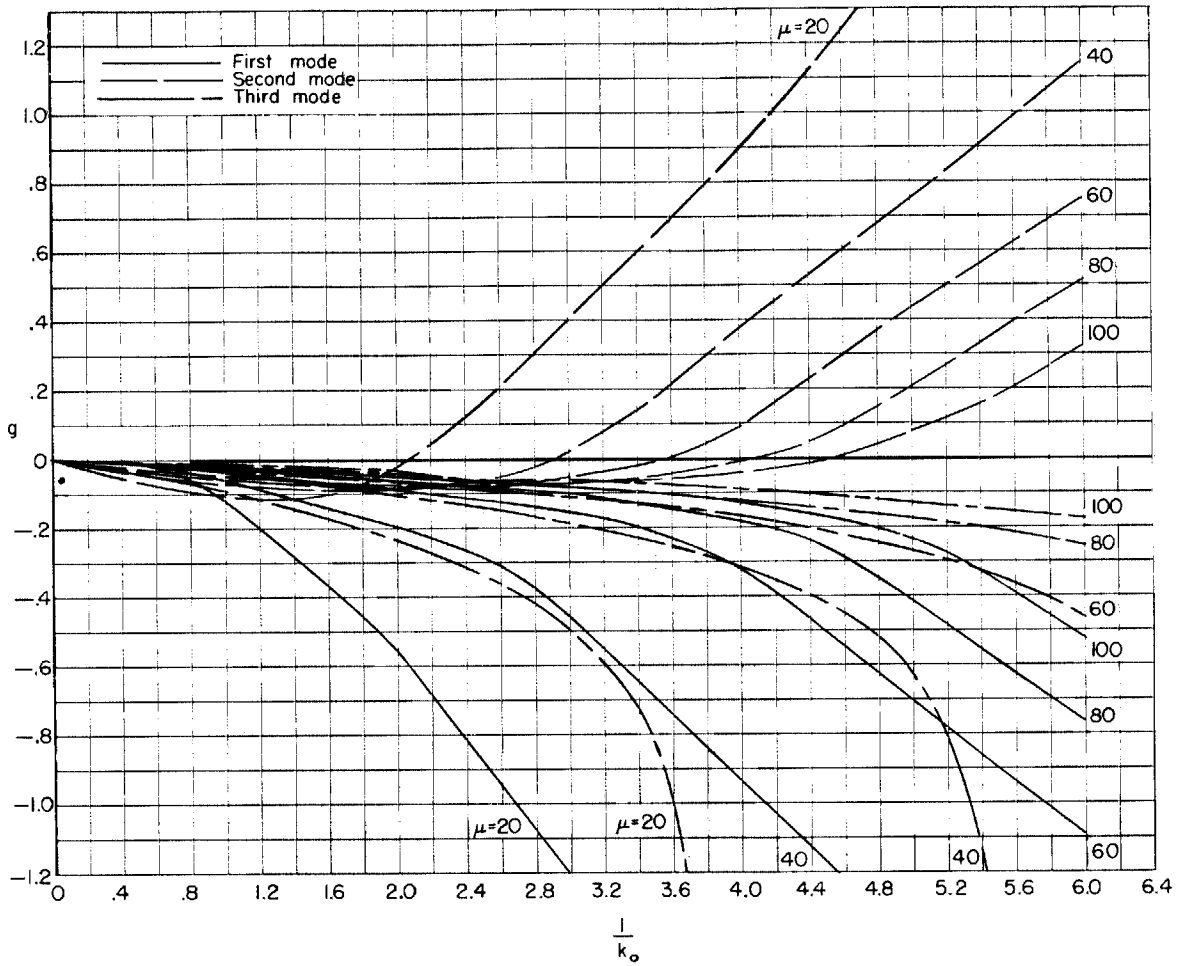

(a) M = 0.

Figure 6.- Damping required for flutter as calculated for mass ratios from 20 to 100 and Mach numbers from 0 to 0.98.

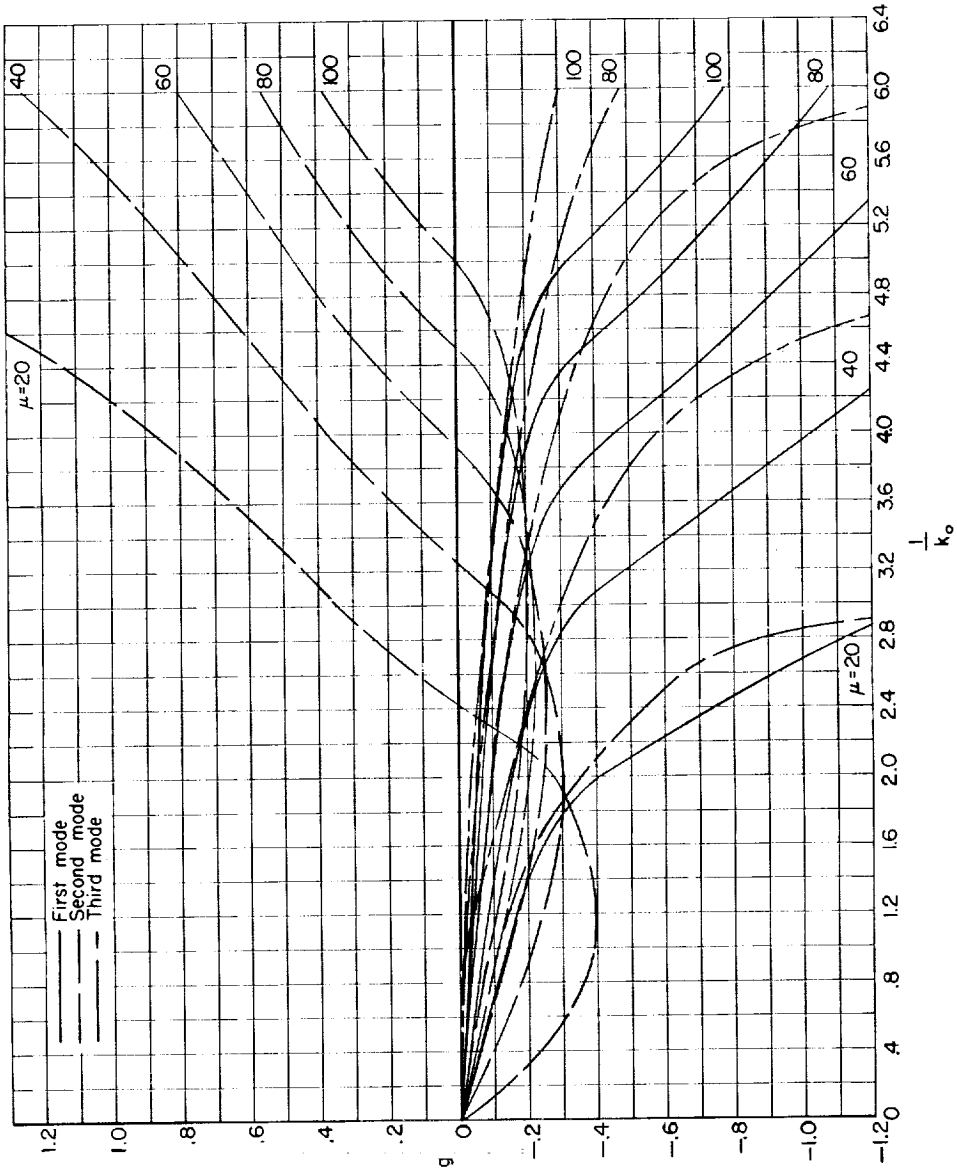

(b) M = 0.75.

Figure 6.- Continued.

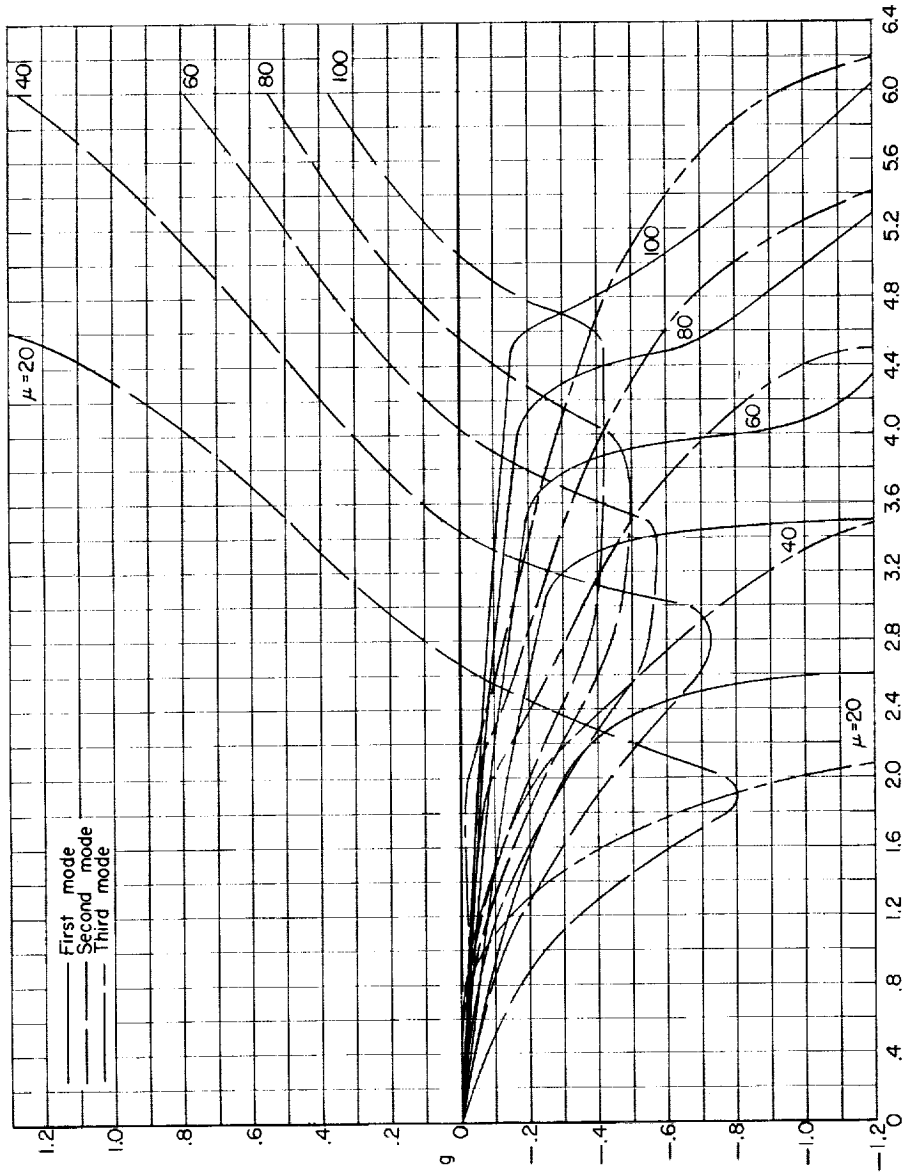

(c) M = 0.90.

Figure 6.- Continued.

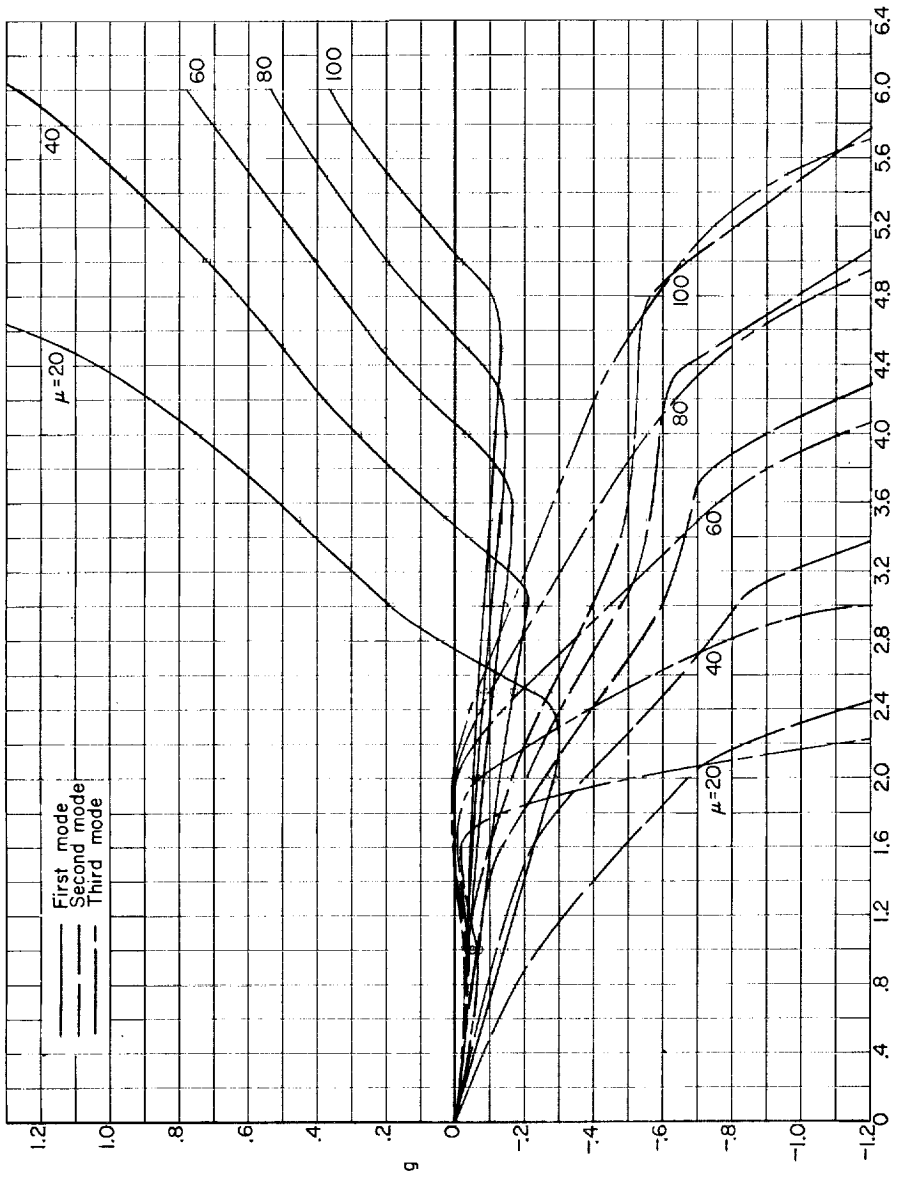

(d) M = 0.92.

Figure 6.- Continued.

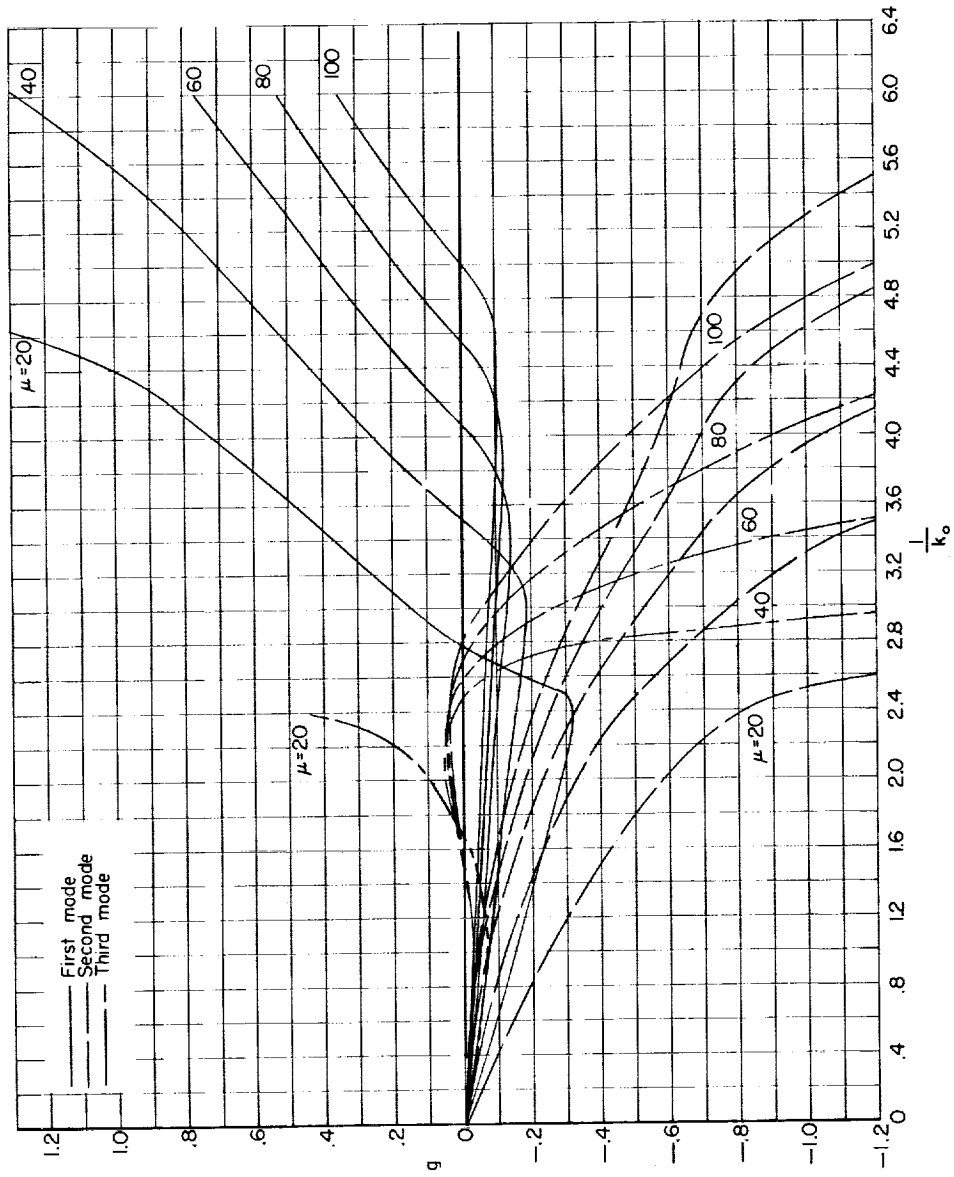

(e) M = 0.94.

Figure 6.- Continued.

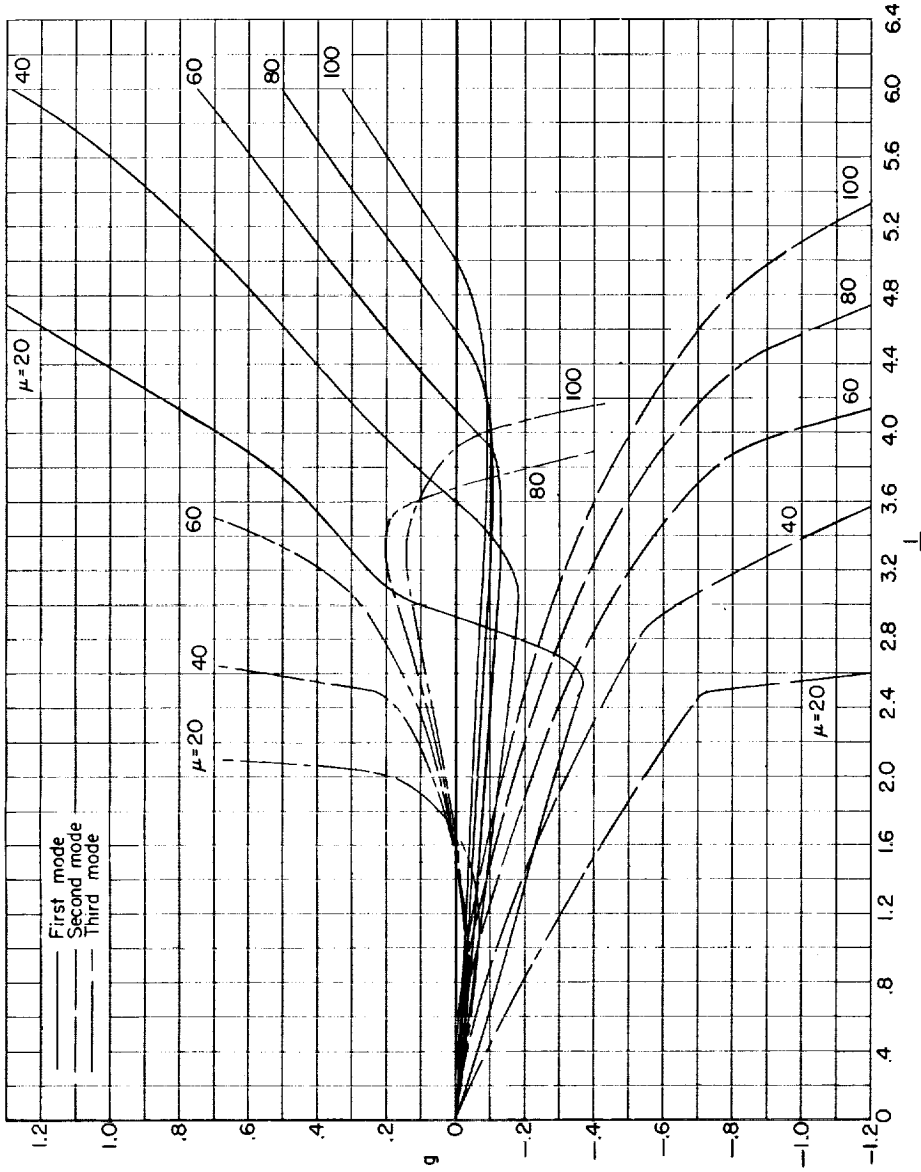

(f) M = 0.96.

Figure 6.- Continued.

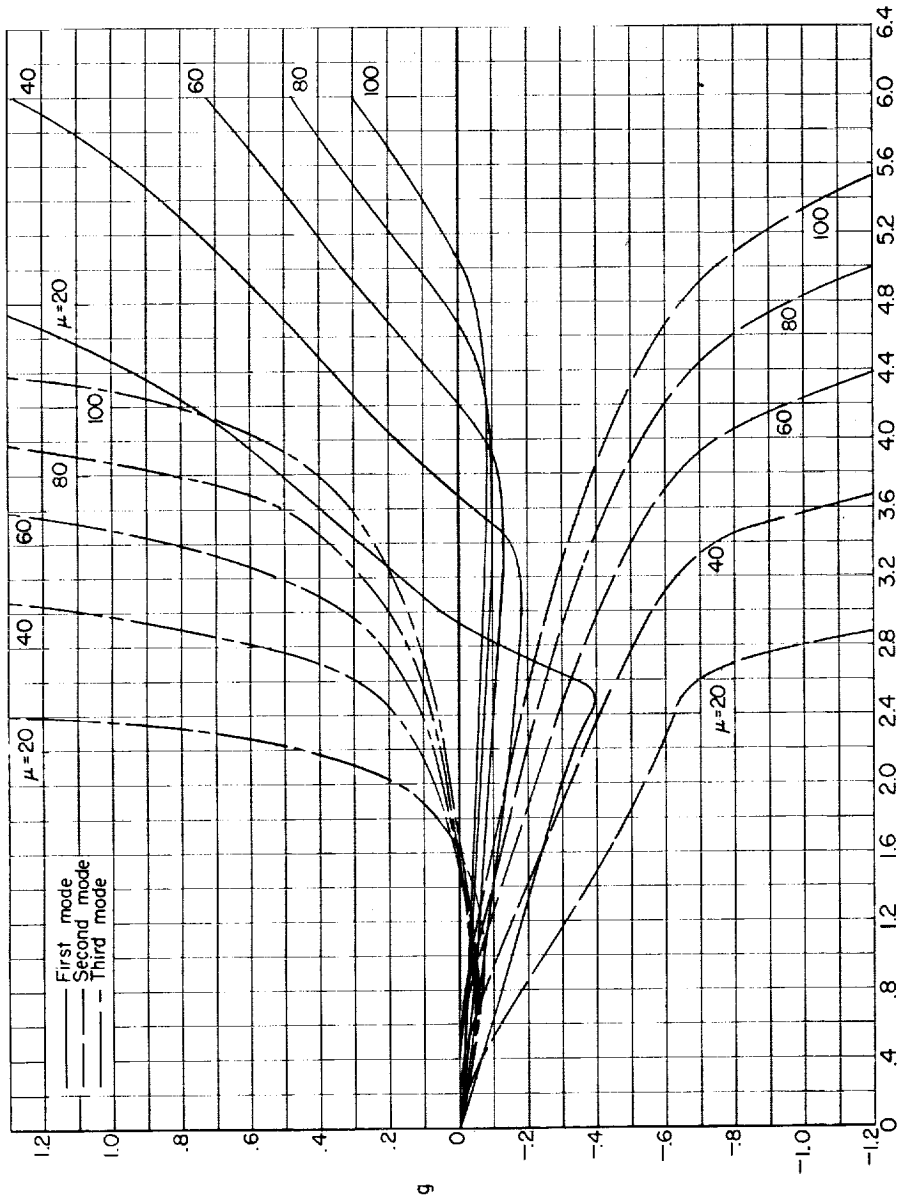

(g) M = 0.98.

Figure 6.- Concluded.

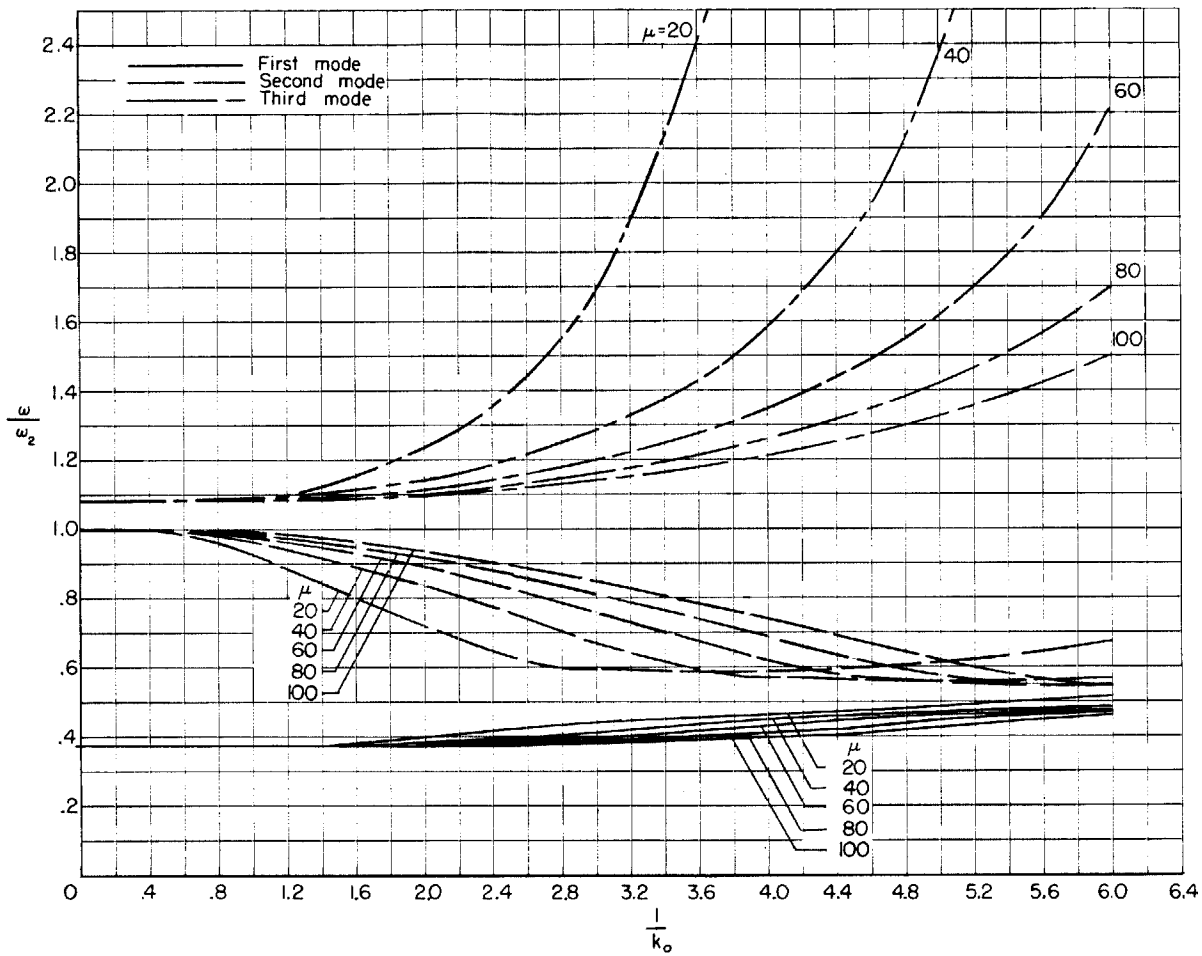

(a) M = 0.

Figure 7.- Frequency ratio $\frac{\omega}{\omega_2}$ as calculated for mass ratios from 20 to 100 and Mach numbers from 0 to 0.98.

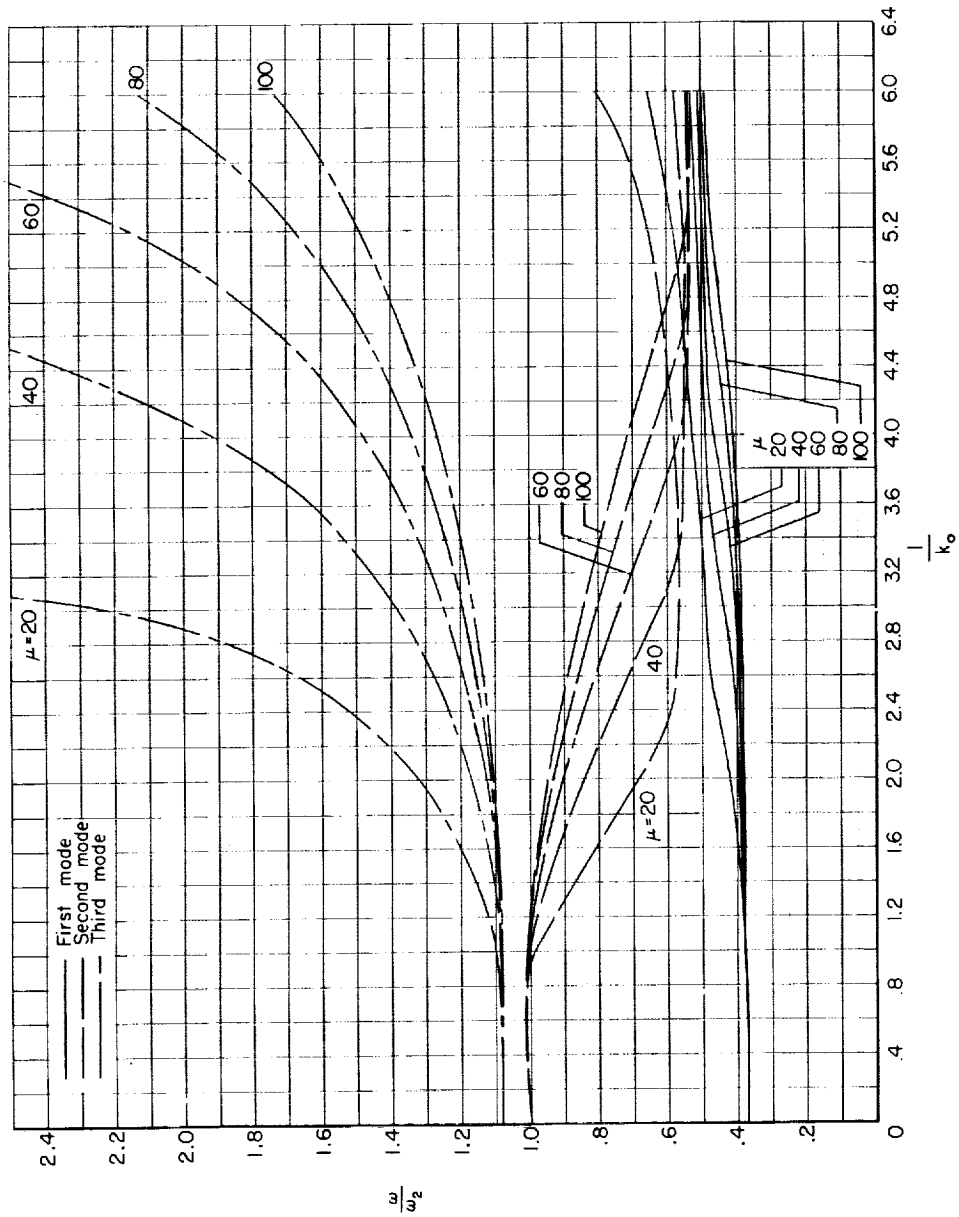

(b) M = 0.75.

Figure 7.- Continued.

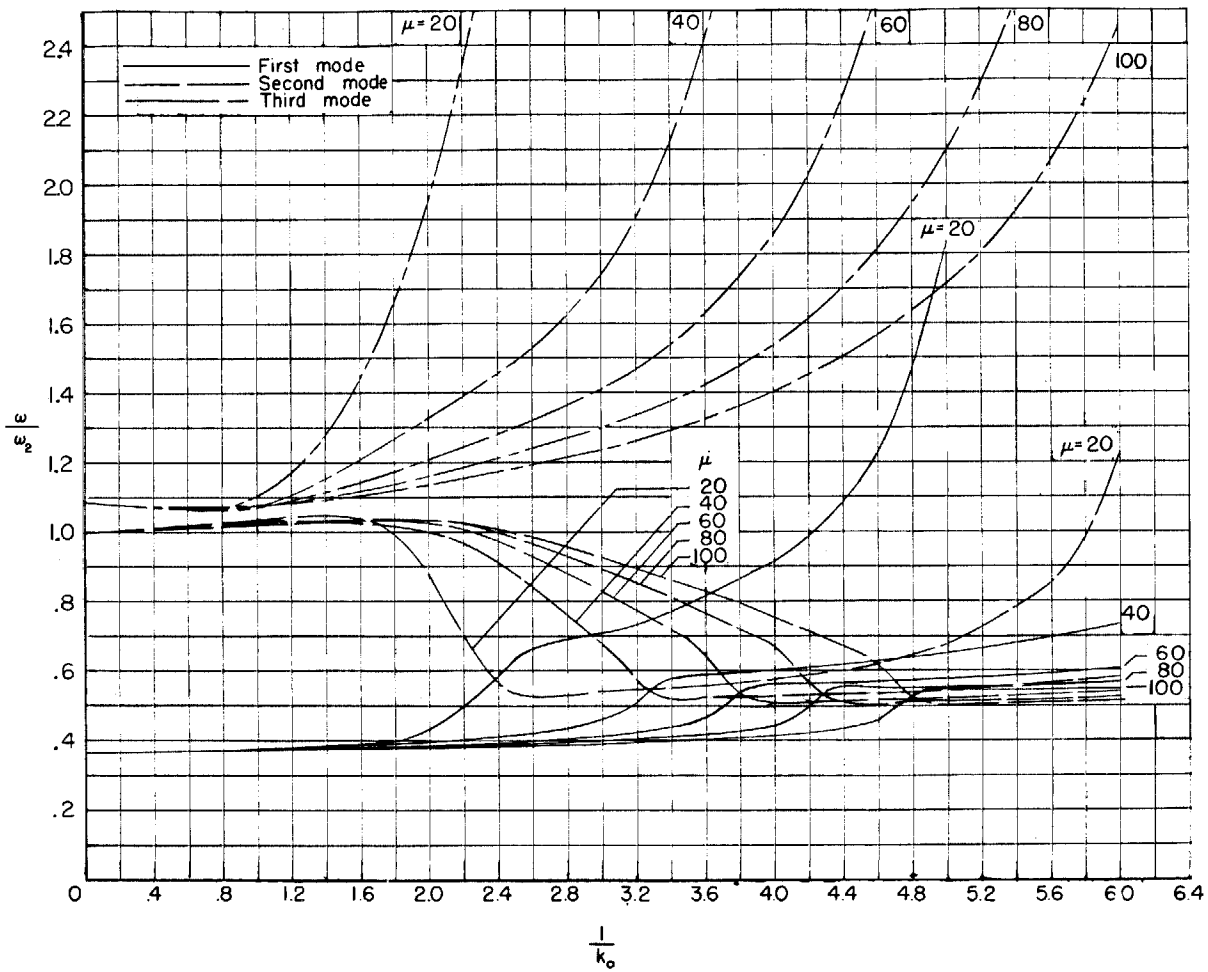

(c) M = 0.90.

Figure 7.- Continued.

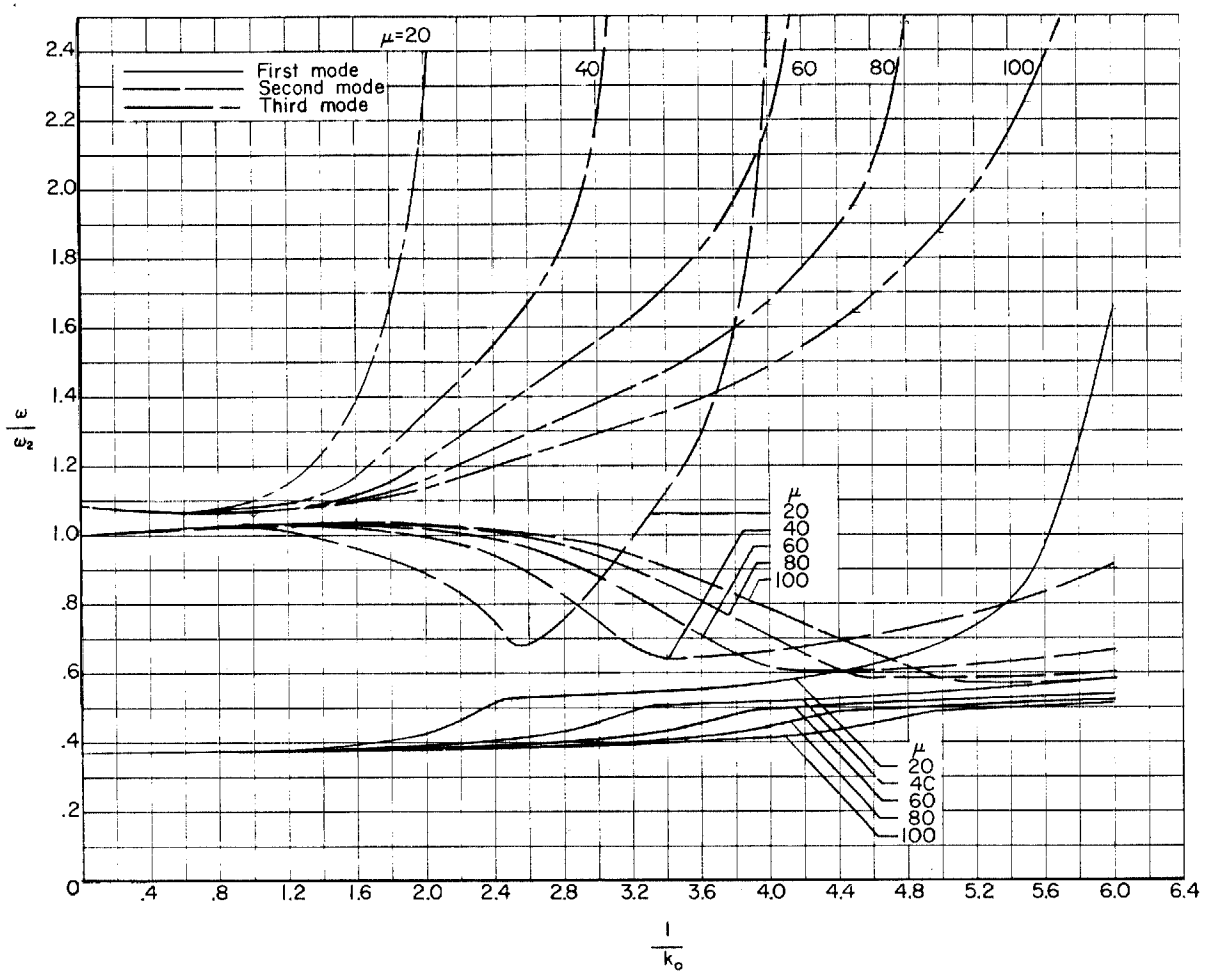

(d) M = 0.92.

Figure 7.- Continued.

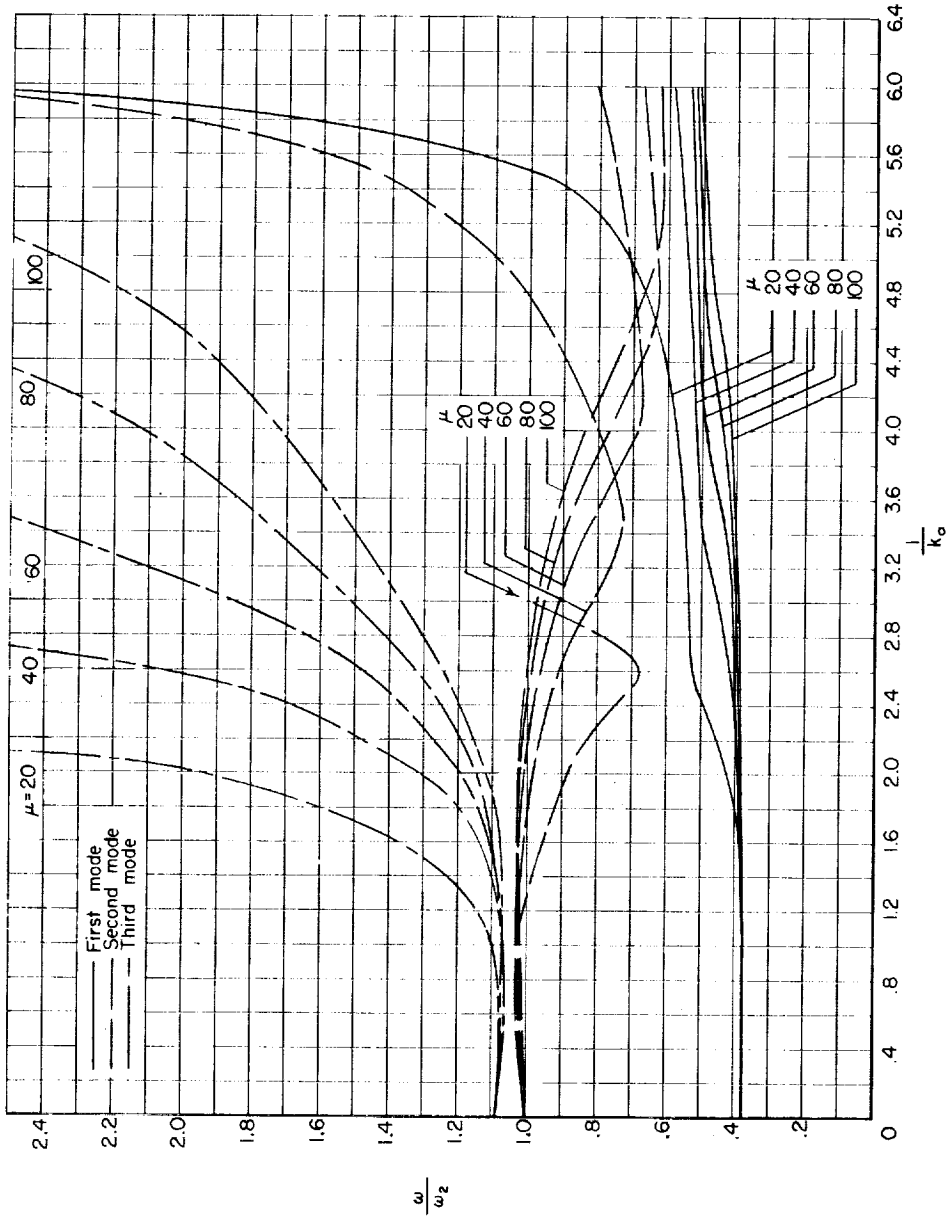

(e) M = 0.94.

Figure 7.- Continued.

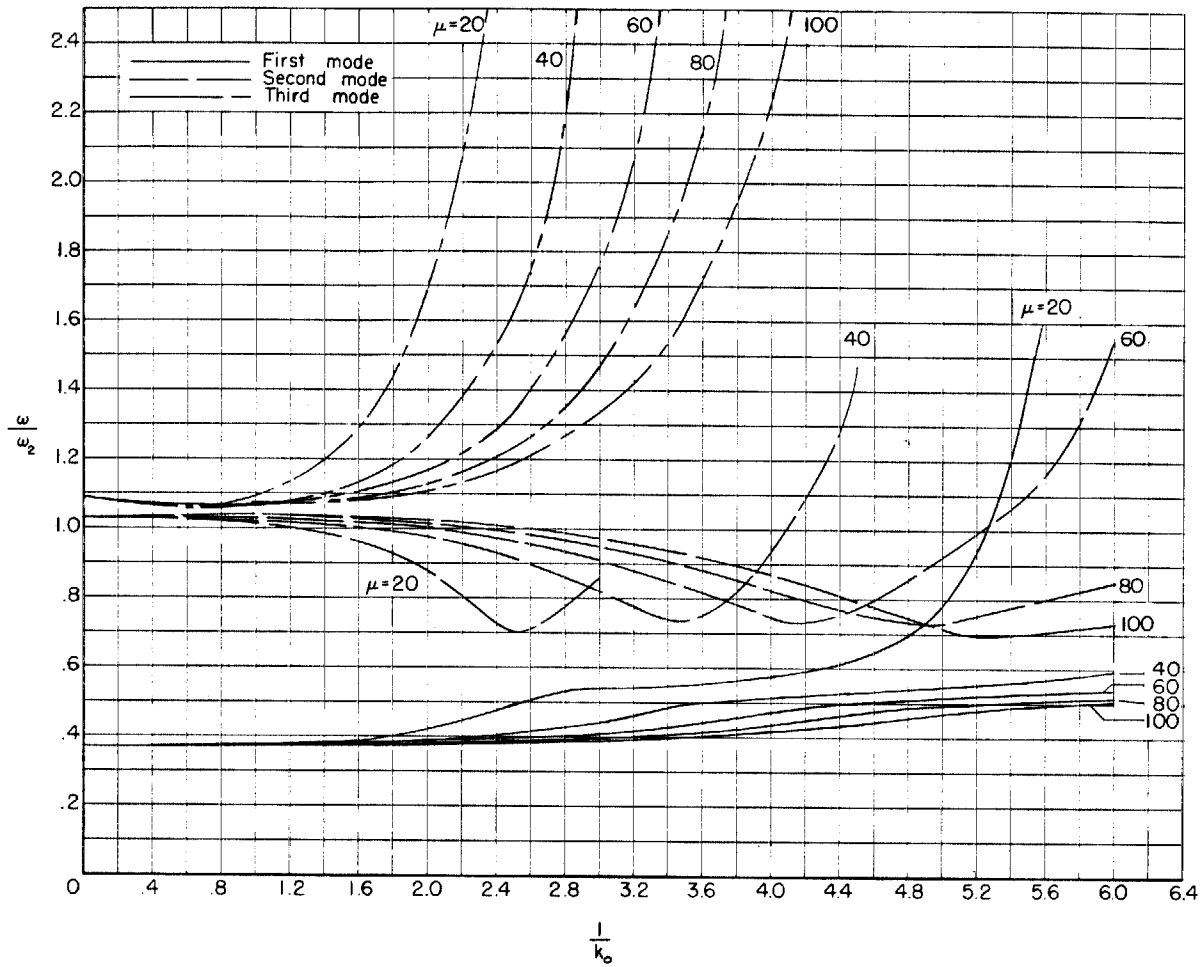

(f) M = 0.96.

Figure 7.- Continued.

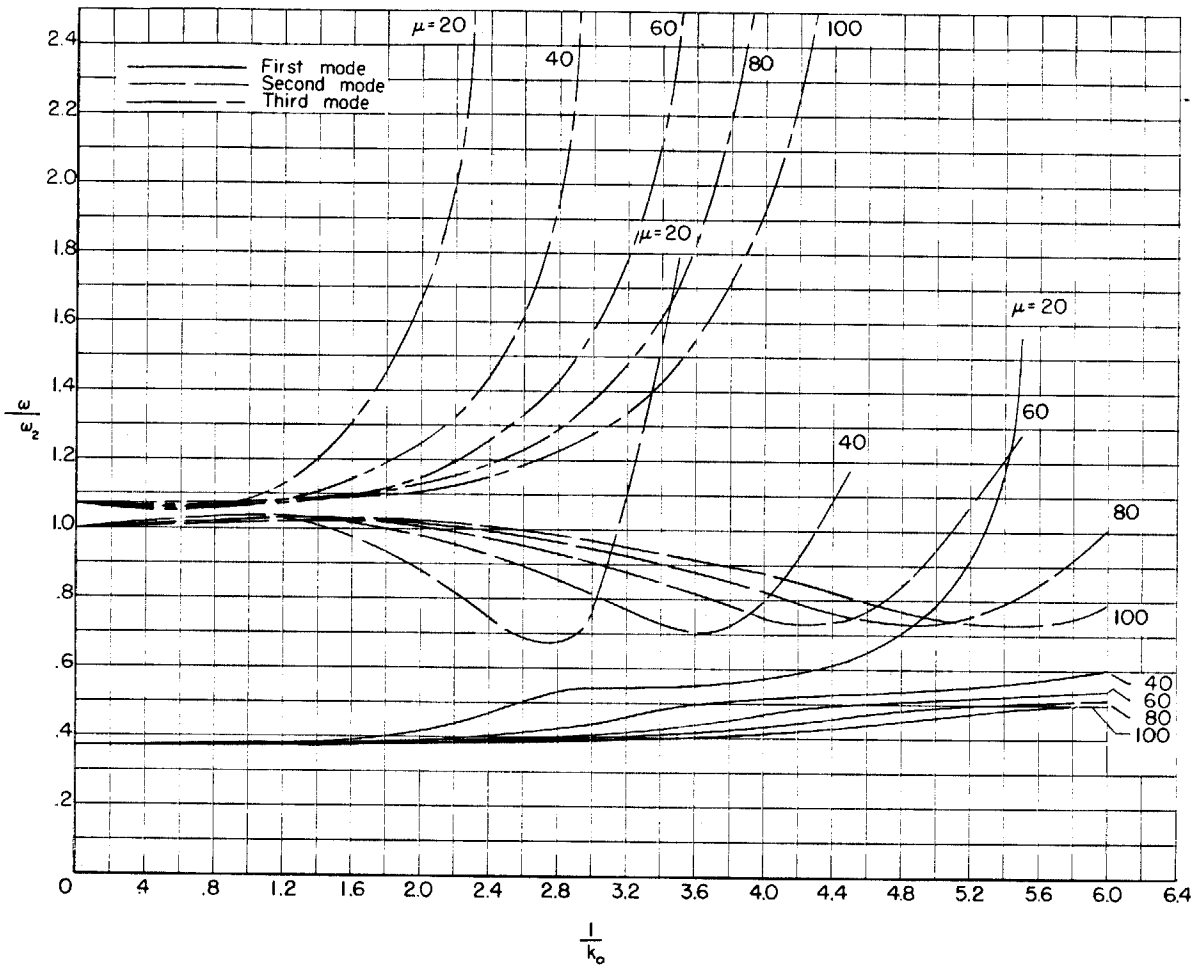

(g) M = 0.98.

Figure 7.- Concluded.

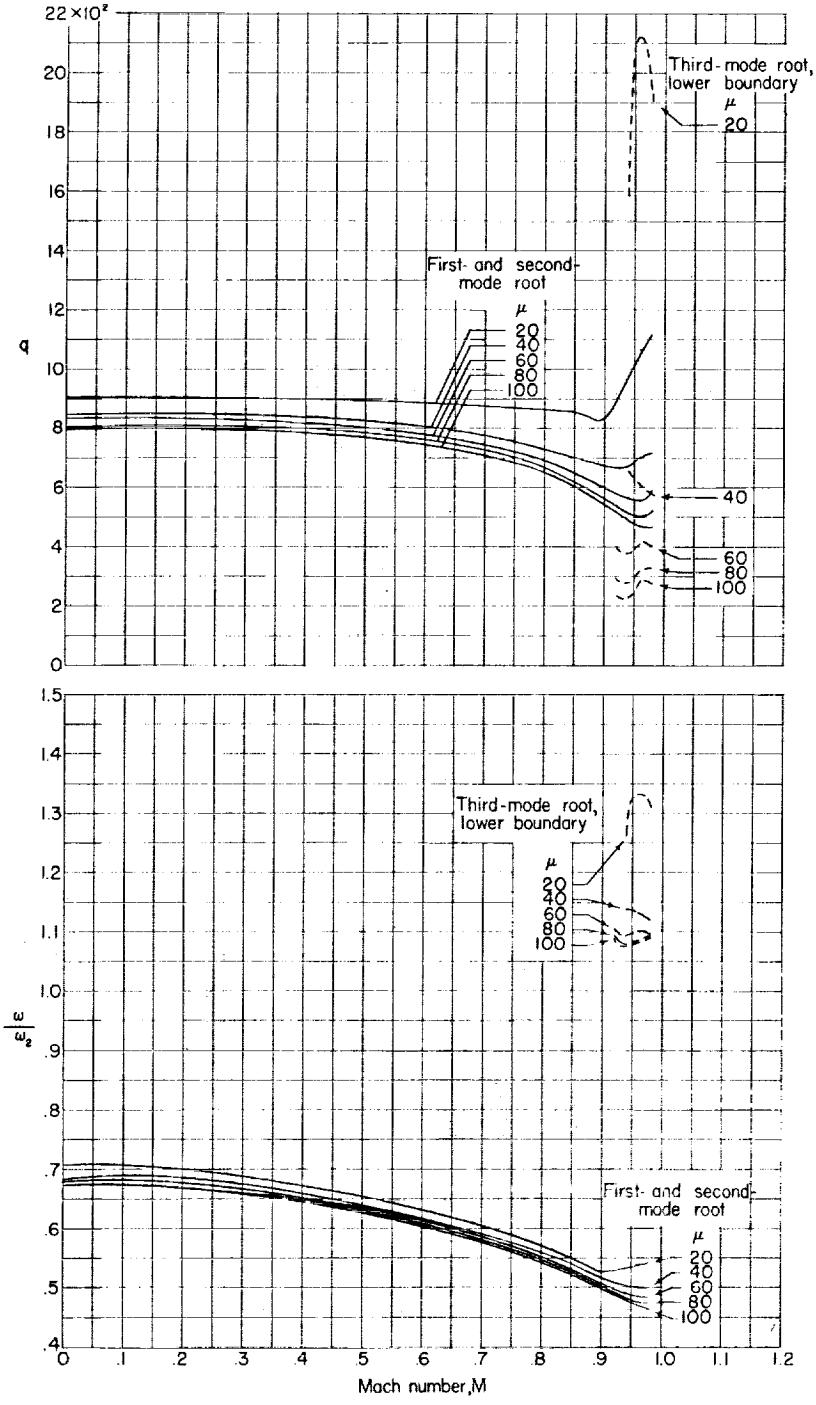

Figure 8.- Effect of mass ratio on the variations of dynamic pressure required for flutter and frequency ratio with Mach number.

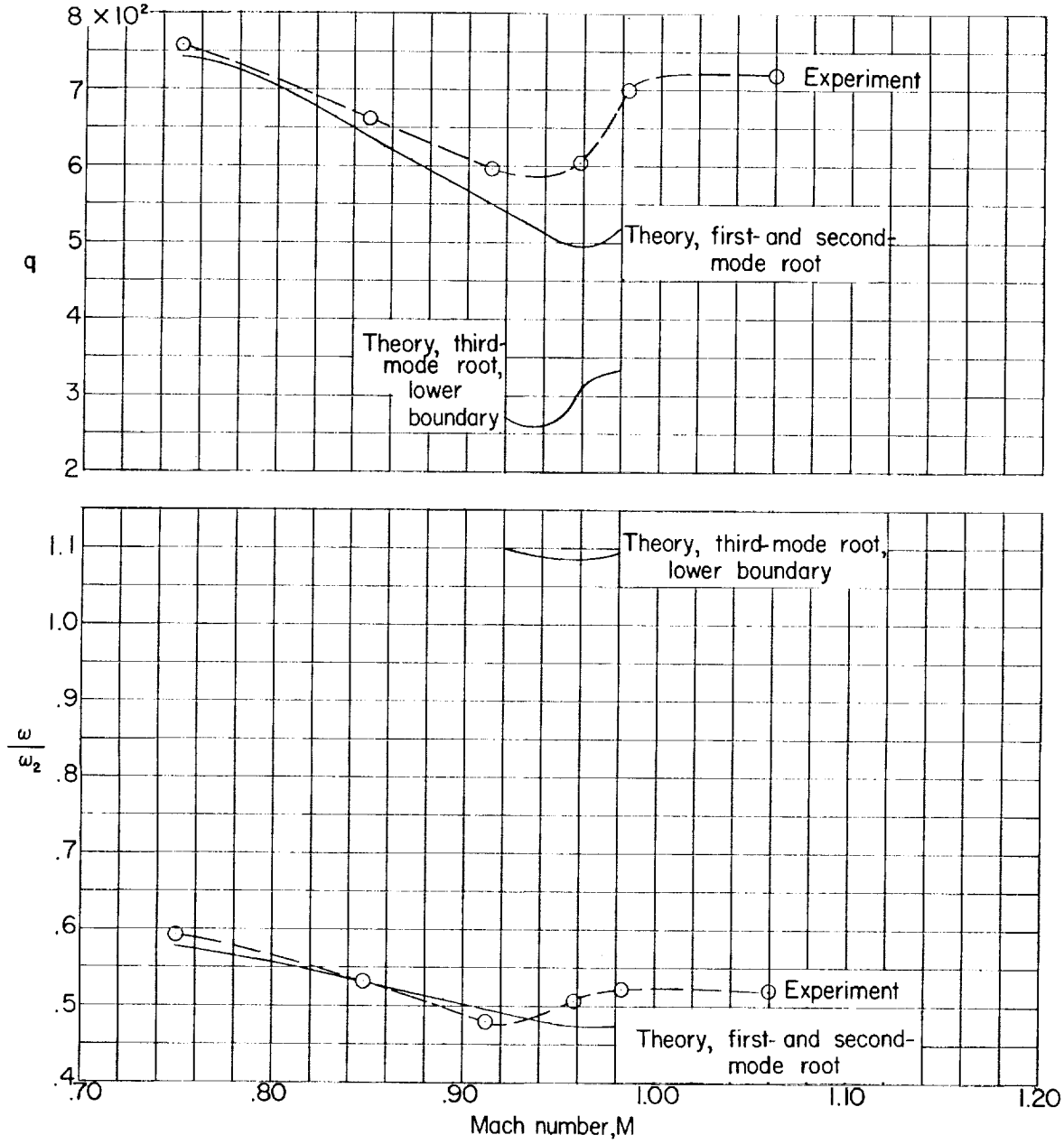

Figure 9.- Comparison of theoretical and experimental flutter boundaries.